Tropospheric Thermal Forcing of the Stratosphere through Quasi-Balanced Dynamics

JONATHAN LIN[a,c] AND KERRY EMANUEL[b]

[a] *Lamont-Doherty Earth Observatory, Columbia University, New York, New York*
[b] *Lorenz Center, Department of Earth, Atmospheric, and Planetary Sciences, Massachusetts Institute of Technology, Cambridge, Massachusetts*
[c] *Department of Earth and Atmospheric Sciences, Cornell University, Ithaca, New York*

(Manuscript received 2 May 2023, in final form 12 December 2023, accepted 27 December 2023)

ABSTRACT: The steady response of the stratosphere to tropospheric thermal forcing via an SST perturbation is considered in two separate theoretical models. It is first shown that an SST anomaly imposes a geopotential anomaly at the tropopause. Solutions to the linearized quasigeostrophic potential vorticity equations are then used to show that the vertical length scale of a tropopause geopotential anomaly is initially shallow, but significantly increased by diabatic heating from radiative relaxation. This process is a quasi-balanced response of the stratosphere to tropospheric forcing. A previously developed, coupled troposphere–stratosphere model is then introduced and modified. Solutions under steady, zonally symmetric SST forcing in the linear β-plane model show that the upward stratospheric penetration of the corresponding tropopause geopotential anomaly is controlled by two nondimensional parameters: 1) a dynamical aspect ratio and 2) a ratio between tropospheric and stratospheric drag. The meridional scale of the SST anomaly, radiative relaxation rate, and wave drag all significantly modulate these nondimensional parameters. Under Earthlike estimates of the nondimensional parameters, the theoretical model predicts stratospheric temperature anomalies 2–3 larger in magnitude than that in the boundary layer, approximately in line with observational data. Using reanalysis data, the spatial variability of temperature anomalies in the troposphere is shown to have remarkable coherence with that of the lower stratosphere, which further supports the existence of a quasi-balanced response of the stratosphere to SST forcing. These findings suggest that besides mechanical and radiative forcing, there is a third way the stratosphere can be forced—through the tropopause via tropospheric thermal forcing.

SIGNIFICANCE STATEMENT: Upward motion in the tropical stratosphere, the layer of atmosphere above where most weather occurs, is thought to be controlled by weather disturbances that propagate upward and dissipate in the stratosphere. The strength of this upward motion is important since it sets the global distribution of ozone. We formulate and use simple mathematical models to show the vertical motion in the stratosphere can also depend on the warming in the troposphere, the layer of atmosphere where humans live. We use the theory as an explanation for our observations of inverse correlations between the ocean temperature and the stratosphere temperature. These findings suggest that local stratospheric cooling may be coupled to local tropospheric warming.

KEYWORDS: Dynamics; Potential vorticity; Vertical motion; Stratosphere-troposphere coupling; Stratosphere; Tropopause

1. Introduction

The Brewer–Dobson circulation (BDC) is a global-scale overturning circulation in the stratosphere, characterized by air that ascends into and within the tropical stratosphere, spreading poleward and eventually downward in the extratropical winter hemisphere. This stratospheric circulation can significantly impact tropospheric climate, most notably through its modulation of the distribution of stratospheric ozone, which absorbs harmful ultraviolet radiation from the sun (Dobson 1956). The widely accepted mechanism that explains the existence of the BDC is the principle of "downward control" (Haynes and McIntyre 1987; Haynes et al. 1991). This principle states that for steady circulations, the upward mass flux across a specified vertical level is solely a function of the zonal momentum sources (wave drag) and sinks above that level; thus, processes in the middle and upper stratosphere can exert a "downward" influence on flow in the lower stratosphere and troposphere. The theoretical findings of Haynes et al. (1991) have been well supported by numerical modeling evidence and withstood the test of time (Butchart 2014, and references therein). Thus, in the "downward control" paradigm, wave dissipation drives the circulation.

The BDC is typically separated into two branches: a slow and deep equator-to-pole overturning branch, and a faster shallow branch in the lower stratosphere extending to about 50° latitude (Plumb 2002; Birner and Bönisch 2011). In this study, references to the BDC refer to the shallow branch circulation. The shallow branch is thought to be driven by subtropical wave dissipation in the lower stratosphere (Plumb and Eluszkiewicz 1999, hereafter PE99; Plumb 2002).

In our opinion, there are a few characteristics of the shallow branch circulation that remain unresolved. First, calculations of residual vertical velocities at 70 hPa indicate off-equator maxima in shallow branch upwelling in the summertime hemisphere (Randel et al. 2008; Seviour et al. 2012). Even though wave drag can force circulations nonlinearly and nonlocally,

Corresponding author: Jonathan Lin, jlin@ldeo.columbia.edu

DOI: 10.1175/JAS-D-23-0081.1

wave drag is at its annual maximum in the winter hemisphere, which is thus at odds with the observation of tropical upwelling maximizing in the summertime hemisphere (Holton et al. 1995; PE99). In fact, all of the experiments performed in PE99 showed that as long as wave drag maximizes in the winter hemisphere, upwelling maximizes in the winter hemisphere. Only when thermal forcing was included, did PE99 observe that upwelling maximizes in the summer hemisphere. Furthermore, at low latitudes, a weak flow-dependent force (such as momentum diffusivity or linear damping) can be of leading-order importance in determining the steady circulation; as PE99 showed, these weak forces, which can arise from thermal forcing, undermine the underlying hypothesis of downward control, namely, that the force can be specified independently of the applied heating. All of this together implies that thermal forcing may be important in determining tropical stratospheric upwelling.

In the tropical stratosphere, the observed upwelling strength is strongly correlated with temperature (Randel et al. 2006; Kerr-Munslow and Norton 2006), since a cold anomaly that slowly varies in time must be maintained by adiabatic cooling against the effect of radiative heating. Therefore, via downward-control arguments, wave dissipation has been historically linked with tropopause temperature. For instance, an annual cycle in subtropical wave dissipation of equatorward-propagating extratropical waves has been suggested as responsible for the annual cycle in tropical tropopause temperature (which is much larger in amplitude than that of the tropical troposphere) (Yulaeva et al. 1994; Holton et al. 1995; Randel et al. 2002; Taguchi 2009; Garny et al. 2011; Kim et al. 2016). Other studies have also attempted to understand how waves originating in the tropics can explain various aspects of the tropopause region, including the annual cycle in temperature (Boehm and Lee 2003; Norton 2006; Randel et al. 2008; Ryu and Lee 2010; Ortland and Alexander 2014; Jucker and Gerber 2017). In this view, the strength of zonally symmetric upwelling in the lower stratosphere is the primary control on zonally symmetric temperature near the tropopause.

In contrast, many observational studies have found that, on a variety of space and time scales, strong cold anomalies occur above regions of deep convection—in essence, local and regional tropopause cooling is associated with local and regional tropospheric (Johnson and Kriete 1982; Gettelman et al. 2002; Dima and Wallace 2007; Holloway and Neelin 2007; Kim and Son 2012; Grise and Thompson 2013; Virts and Wallace 2014; Kim et al. 2018). There also seems to be some spatial correlation between tropospheric warming and stratospheric cooling trends on global warming time scales (see Fig. 1 of Fu et al. 2006). In general, the cold anomalies in the lower stratosphere have been interpreted to be caused by convection itself, or forced from the "bottom up." Since convection warms the troposphere, there is strong observational evidence of an anticorrelation between tropospheric temperature and lower-stratospheric temperature.

This oft-observed link between tropopause cooling and tropospheric warming has a number of theoretical explanations. First, there is the hypothesis that convective overshooting (of the level of neutral buoyancy) can cool the tropopause (Danielsen 1982; Sherwood 2000; Kuang and Bretherton 2004), emphasizing the role of convection in determining the mean temperature of the tropopause. Holloway and Neelin (2007) offer an alternative hypothesis, and propose that a convective cold top forms via hydrostatic adjustment above tropospheric convective heating. This theory requires that the associated pressure perturbation vanishes at some arbitrary level. Note that there is no dependence of the temperature anomaly on the horizontal scale in this theory. Separately, some authors have also argued that deep convection can excite a large-scale Kelvin wave response, which also has a vertically tilted signature of tropopause cooling (Kiladis et al. 2001; Randel et al. 2003). Finally, the anticorrelation in tropospheric temperature and lower-stratospheric temperature has also been explained through the vertical propagation of Rossby waves (Dima and Wallace 2007; Grise and Thompson 2013), though this theory is focused on subtropical regions, rather than on the deep tropics. Regardless, most of these studies focus on daily to monthly time scales, and do not consider how the observed lower-stratospheric cold anomalies might affect lower-stratospheric upwelling more broadly. This is not trivial—while changes to the tropopause temperature that project onto the zonal mean could theoretically induce changes in shallow branch upwelling, a corresponding, self-consistent change in the momentum budget must also occur to balance the changes in the meridional circulation (Ming et al. 2016a).

If one persists with the assumption that the same mechanism responsible for local- and regional-scale anticorrelations between tropospheric warming and tropopause cooling can manifest itself at the zonally symmetric scale (which is not a given), then it is perhaps unsurprising that there also exists a tight coupling between tropospheric warming and the BDC shallow branch mass flux, at least when using SST to characterize the tropical troposphere. In general circulation models (GCMs) and reanalyses, there are strong correlations between tropical-mean SST and the BDC shallow branch mass flux, across a wide variety of time scales (Lin et al. 2015; Orbe et al. 2020; Abalos et al. 2021). Fluctuations in tropical stratospheric upwelling have also been tied to El Niño–Southern Oscillation (ENSO), one of the dominant sources of interannual tropical SST variability (Randel et al. 2009). In fact, interannual variations in tropical mean SST explain 40%–50% of the interannual variability of the 70-hPa vertical mass flux (Lin et al. 2015; Abalos et al. 2021). In addition, nearly 70% of the CMIP6 model spread in the long-term trend of shallow branch mass flux is explained by the spread in tropical warming (Abalos et al. 2021).

The tight coupling between tropical SST and BDC shallow branch upwelling on interannual to climate change time scales has been explained through changes to the wave drag, in light of the downward-control paradigm: surface warming leads to upper-tropospheric warming and modification of the subtropical jets, which alters the upward propagation and dissipation of midlatitude waves in the subtropics (Garcia and Randel 2008; Calvo et al. 2010; Shepherd and McLandress 2011; Lin et al. 2015). While these theories can explain how SST and shallow branch mass flux are correlated, they were not constructed to also explain the oft-observed local-scale anticorrelation between SST and tropopause temperature.

In this study, we put forth an alternative explanation for the anticorrelation between tropospheric and lower-stratospheric temperature. To start, consider the simplified atmospheric state shown in Fig. 1, which has a troposphere in radiative convective equilibrium, with an overlying stratosphere at rest. Here, we assume that the tropopause acts as an infinitesimally small boundary between the troposphere and stratosphere, which neglects the existence of the tropical tropopause layer (TTL) (Fueglistaler et al. 2009), as further discussed in the conclusions. The TTL's role in the broader climate should not be neglected, especially since the TTL temperature has been linked with the concentration of water vapor in the stratosphere (Jensen and Pfister 2004; Fueglistaler et al. 2005; Randel et al. 2006; Randel and Park 2019).

This approximation notwithstanding, suppose we impose a steady patch of positive SST anomaly in the ocean. The increased surface enthalpy flux warms the troposphere, following a moist adiabat. The surface pressure falls, and the geopotential at the tropopause rises. Since there cannot be a pressure discontinuity across the tropopause, the pressure must also rise in the lower stratosphere. How far up does it extend, and what is the steady response in the stratosphere?

Section 2 tries to answer this conceptual question by introducing the concept of SST forcing of the tropopause and building a zonally asymmetric framework to understand the processes that control the upward extent of tropopause anomalies. It is shown that there is a quasi-steady, quasi-balanced response of the stratosphere to tropospheric thermal forcing. Section 3 extends the analysis to the zonally symmetric case, using a steady, coupled troposphere–stratosphere system to show how zonally symmetric SST anomalies (or zonally symmetric tropospheric heating) can influence tropical upwelling in the lower stratosphere. Section 4 uses reanalysis data to argue for the real-world presence of the processes described in the proposed theory. Section 5 concludes the study with a summary and discussion.

2. Stratospheric response to a tropopause anomaly

In this section, we introduce a simple conceptual model that will 1) illuminate how SST forcing can induce a tropopause geopotential anomaly and 2) understand what parameters modulate the upward extent of the tropopause anomaly into the stratosphere.

To understand how the stratosphere could be forced by the troposphere, we begin with tropospheric dynamics. In radiative–convective equilibrium, a valid approximation is that of strict convective quasi equilibrium, where the saturation moist entropy s^* is constant with height (Emanuel 1987; Emanuel et al. 1994). Emanuel (1987) showed that linearized geopotential perturbations are directly connected to linearized s^* perturbations (note here, for simplicity, we have ignored the small effect of water vapor on density):

$$\frac{\partial \phi'}{\partial p} = -\left(\frac{\partial T}{\partial p}\right)_{s^*} s^{*\prime}, \tag{1}$$

where prime superscripts indicate perturbation quantities. Since s^* is constant with height, Eq. (1) can be directly integrated in pressure to yield (as also shown in Lin and Emanuel 2022)

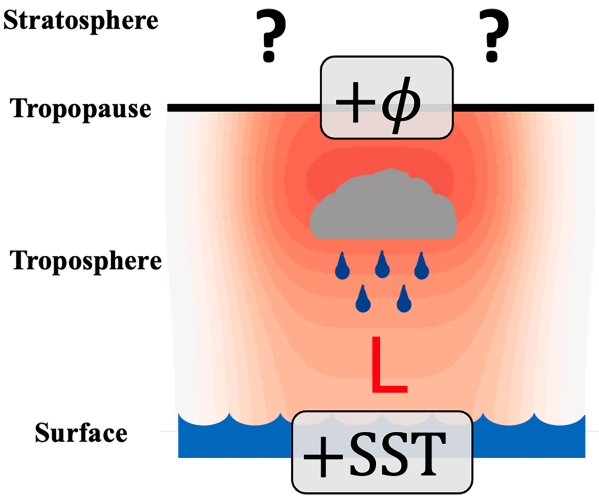

FIG. 1. Schematic of a troposphere in radiative–convective equilibrium, with an overlying stratosphere that is at rest. The troposphere is forced with a steady warm SST anomaly in the ocean. The troposphere warms (indicated by color shading) following a moist adiabat, the surface pressure falls, and the geopotential rises at the tropopause. How does the stratosphere respond to an imposed tropopause geopotential anomaly?

$$\phi'(p) = \phi'_b + s^{*\prime}[\overline{T}_b - \overline{T}(p)], \tag{2}$$

where ϕ'_b is the perturbation boundary layer geopotential, $\overline{T}$ is the basic-state temperature, and $\overline{T}_b$ is the basic-state boundary layer temperature. We nondimensionalize according to

$$\phi \to H^2N^2\phi \quad \text{and} \quad s^* \to \frac{H^2N^2}{\overline{T}_b - [\overline{T}]}s^*, \tag{3}$$

where H is the scale height, N^2 is the buoyancy frequency, and $[\overline{T}]$ is the basic-state vertically averaged temperature. Dropping primes for perturbation quantities and nondimensionalizing yields

$$\phi(p) = \phi_b + [1 - V_1(p)]s^*, \tag{4}$$

where V_1 is the nondimensional first baroclinic mode (Lin and Emanuel 2022):

$$V_1(p) = \frac{\overline{T}(p) - [\overline{T}]}{T_b - [\overline{T}]}. \tag{5}$$

Equation (5) shows that the first baroclinic mode is positive near the surface, transitions to zero in the midtroposphere, and is negative at the tropopause (which is evaluated at a fixed pressure). Evaluating Eq. (4) at the tropopause yields

$$\phi(\hat{p}_t) = \phi_0 - V_1(\hat{p}_t)s^*, \tag{6}$$

where $\hat{p}_t$ is the nondimensional tropopause pressure, and $\phi_0 = \phi_b + s^*$ is the barotropic geopotential. Note that the

barotropic geopotential is constant with height. The total geopotential is the linear sum of the contributions of the tropospheric barotropic and baroclinic geopotential.

Since the tropopause is colder than the mean troposphere temperature, $V_1(\hat{p}_t)$ is negative, such that for positive SST anomalies ($s^{*'} > 0$), the tropopause geopotential anomaly will also be positive, provided the barotropic geopotential is not less than $V_1(\hat{p}_t)s^*$. In the real atmosphere, baroclinic perturbations are typically around an order of magnitude larger than barotropic ones (Lin and Emanuel 2022), such that for the sake of simplicity, we proceed with the approximation that ϕ_0 is small in relation to the baroclinic term. We will relax this assumption in the next section. Then, in this simple conceptual framework, we have a warm patch of ocean that imposes a steady positive geopotential anomaly at the tropopause.

Next, we will consider what happens to the stratosphere subject to a steady tropopause forcing (i.e., a steady lower boundary condition). The response of the stratosphere to external forcing has been well-studied using theoretical models (see Garcia 1987; Haynes et al. 1991; PE99, among many others). However, the external forcing is typically presented in terms of being mechanical (wave driven) or thermal in origin. We instead impose a tropopause forcing via the SST anomaly, and use the well-known quasigeostrophic potential vorticity equations (QGPV), linearized about a resting basic state on an f plane:

$$q'(x, y, z) = \frac{1}{f_0}\nabla_H^2\phi' + \frac{f_0}{N^2}\frac{\partial^2\phi'}{\partial z^2} - \frac{f_0}{HN^2}\frac{\partial\phi'}{\partial z}, \tag{7}$$

where q is the potential vorticity (PV), f_0 is the Coriolis parameter, N is the buoyancy frequency, and ϕ is the geopotential. Here, we are considering perturbations large enough in scale for the quasigeostrophic approximation to apply. Dropping primes for perturbation quantities, assuming wavelike solutions in the zonal and meridional [$\exp(ikx + ily)$], and nondimensionalizing by

$$\begin{aligned} &x \to Lx, \quad y \to Ly, \quad z \to Hz, \\ &\phi \to H^2N^2\phi, \quad q \to f_0 q, \quad t \to t/f_0, \end{aligned} \tag{8}$$

where $L = NH/f$ is the Rossby radius of deformation, we obtain

$$\left[\frac{\partial^2}{\partial z^2} - \frac{\partial}{\partial z} - (k^2 + l^2)\right]\phi = q(z). \tag{9}$$

These equations can be found in most standard textbooks, e.g., section 5.4 of Vallis (2017). Here, we emphasize the boundary conditions:

$$\phi(z = 0) = \phi_T, \tag{10}$$

$$\frac{\partial\phi}{\partial z}(z = \infty) = 0, \tag{11}$$

where the bottom boundary condition enforces continuity of pressure across the tropopause, given the aforementioned tropopause geopotential anomaly that is imposed by an SST anomaly. The upper boundary condition requires that the temperature anomaly (or vertical velocity anomaly) be zero. Though ϕ_T is imposed by the troposphere, via Eq. (6), in reality, barotropic motions are coupled to the stratosphere. Thus, we can only assume the geopotential as a steady lower boundary condition, and solve for the stratosphere in isolation, since we ignored the barotropic geopotential. As shall be illuminated in the next section, the barotropic mode should really be coupled to the stratospheric circulation.

We proceed by considering the stratospheric response to a geopotential anomaly at the tropopause, with zero perturbation PV throughout the rest of the stratosphere. Since imposing a geopotential anomaly at the tropopause has no direct effect on stratospheric PV, it can be considered as the fast stratospheric response to a tropopause geopotential anomaly. In this textbook case, the solution is straightforward:

$$\phi(z) = \exp(m_- z), \tag{12}$$

where

$$m_- = \frac{1 - \sqrt{1 + 4(k^2 + l^2)}}{2}, \tag{13}$$

which shows that the geopotential anomaly decays in the vertical with a scale inversely proportional to the horizontal scale of the anomaly. On redimensionalization, the Rossby penetration depth,

$$R_d = \frac{f_0 L}{N}, \tag{14}$$

where L is the Rossby deformation radius, is the operative vertical scale of the geopotential. Tropopause anomalies with large horizontal scales will extend deeper into the stratosphere than smaller ones.

The temperature anomaly, scaling with $\partial\phi/\partial z$, will also decay exponentially with height according to R_d. But how large can the temperature anomalies get? Thermal wind balance dictates that

$$g\frac{\partial \ln T}{\partial y} = -f\frac{\partial u}{\partial z}. \tag{15}$$

If we take ∂z to scale as the Rossby penetration depth, then we obtain

$$\ln T \approx \frac{\mathrm{Nu}}{g}. \tag{16}$$

Note that f drops out, which indicates that the temperature in the stratosphere does not directly depend on f. It rather depends on the magnitude of the tropopause anomaly, as well as the stratospheric stratification. For the case of zero perturbation PV in the stratosphere, the temperature anomaly is just the geopotential anomaly multiplied by m_-, which is inversely proportional to the horizontal scale of the tropopause PV anomaly. Therefore, the magnitude of the tropopause temperature perturbations can be large for small horizontal-scale

anomalies, though these will be confined to a rather shallow vertical layer near the equator (and may also not obey the quasigeostrophic approximation).

Next, it is instructive to consider how the stratosphere responds to the temperature anomalies. As alluded to earlier, temperature anomalies disturb the radiative equilibrium of the stratosphere. This must be associated with radiative heating anomalies. In this case, PV is no longer conserved. The response of the stratosphere can be modeled as

$$\frac{\partial q}{\partial t} = \frac{f_0}{N^2}\frac{\partial \dot{Q}}{\partial z}, \tag{17}$$

where $\dot{Q}$ is the heating rate (thermal forcing), and is parameterized to be a simple Newtonian radiative relaxation:

$$\dot{Q} = -\alpha_r \frac{\partial \phi}{\partial z}; \tag{18}$$

$\alpha_r > 0$ is the inverse time scale of the Newtonian radiative relaxation. Hitchcock et al. (2010) found that linear radiative relaxation can explain around 80% of the variance in longwave heating rates in a climate model, though this is less accurate in the lower stratosphere, and dependent on the relaxation rate having a height dependence. Nondimensionalizing using Eq. (8), we obtain

$$\frac{\partial q}{\partial t} = -\gamma \frac{\partial^2 \phi}{\partial z^2}, \tag{19}$$

where $\gamma = \alpha_{\text{rad}}/f_0$.

The effect of radiative damping on stratospheric circulations has been thoroughly explored in a number of early theoretical studies (Garcia 1987; Haynes et al. 1991; Haynes and Ward 1993). In particular, the seminal work of Haynes et al. (1991) showed that in zonally symmetric, radiatively damped, time-dependent systems whereby a steady mechanical forcing is instantaneously applied, there is an adjustment to a barotropic state (in u) above the level of forcing. Our setup is similar to the model outlined in section 3 of Haynes et al. (1991), except here the steady forcing is restricted to the tropopause geopotential—the forcing is neither wave driven nor thermal in origin.

To solve for the geopotential, the Green's function (see the appendix) is convoluted with the source term under the lower boundary condition:

$$q_T = -k_m \phi_T, \tag{20}$$

where $k_m = k^2 + l^2$ is the total wavenumber. This can be calculated numerically (see the appendix for more details). Figure 2 shows the stratospheric geopotential solutions that describe the initial and final states after imposing a tropopause geopotential anomaly. The initial geopotential distribution from the steady geopotential anomaly is shown as ϕ_b, and is just the zero interior perturbation PV solution mentioned earlier in the text, where the response decays exponentially with height. The geopotential distribution associated with the generation of anomalous PV through diabatic heating by radiative relaxation is shown in ϕ_q, while the total geopotential is shown as $\phi = \phi_q + \phi_b$. The total geopotential is constant with height (barotropic) above the level of forcing, as found by Haynes et al. (1991).

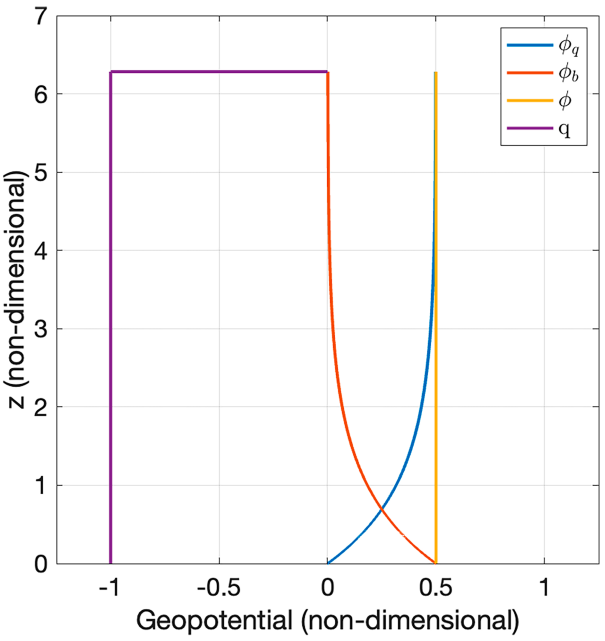

FIG. 2. The geopotential associated with a boundary PV anomaly of $q = -1$ (ϕ_b) (red), a constant PV anomaly of $q = -1$ in the interior (ϕ_q) (blue), and the sum of the two ($\phi = \phi_q + \phi_b$) (yellow). The corresponding total PV is shown in purple. Here we assume $k_m = 2$, and $z_{\text{top}} = 1 + 2\pi$.

A simple physical picture is painted with this conceptual model that can provide a rather straightforward answer to the schematic shown in Fig. 1. If the troposphere is forced with a steady positive SST anomaly, a positive geopotential anomaly forms at the tropopause. A positive tropopause geopotential anomaly is initially accompanied with a cold anomaly in the stratosphere, which is associated with radiative heating and rising motion. If this process is allowed to proceed toward a steady state back to radiative equilibrium, the geopotential and PV must eventually become constant with height (i.e., barotropic), as implied by Eq. (18), and the temperature anomaly in the stratosphere disappears. In this way, the troposphere can force the stratosphere, at least on the steady time scales considered here. This also shows that the geopotential does not have to go to zero at the upper boundary. The only requirement is that the energy density goes to zero. Thus, the assumption of the geopotential going to zero at the upper boundary in Holloway and Neelin (2007) seems arbitrary.

How long does it take to reach the barotropic state? Haynes et al. (1991) showed that in the zonally symmetric case, the adjustment toward a barotropic state above the level of forcing occurs with an upward propagation speed of $w_\alpha = \alpha_{\text{rad}} R_d^2/H_s$. In the tropics, w_α is small, owing to the smallness of both α_{rad} and R_d. For an anomaly of horizontal scale around 5000 km at a latitude of 10°, and a radiative relaxation time scale of $\alpha_{\text{rad}} = 20$ days^{-1},

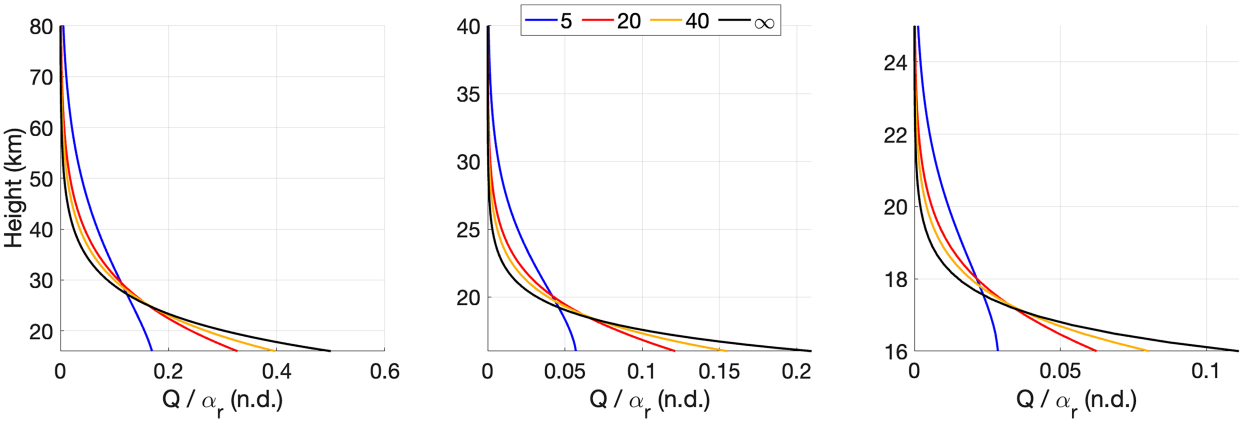

FIG. 3. (left) The diabatic heating profile (Q/α_r) with height in the stratosphere after 30 days of integration, subject to a steady tropopause boundary forcing with a horizontal scale of around 28 000 km, and 5 (blue), 20 (red), and 40 days (yellow). The vertical derivative of the geopotential for the zero-PV stratospheric response to a tropopause forcing (infinite radiative relaxation time scale) is shown in black. (center),(right) As in the left panel, but for a horizontal scale of around 9500 and 4500 km, respectively. We assume a latitude of 10°, a scale height of 8 km, and a tropopause height of 16 km to convert to dimensional height. Note the vertical scale varies in each subplot for detail.

$w_\alpha \approx O(10^{-1})$ mm s^{-1}—an upward propagation of only a few kilometers per year. It is also possible to numerically calculate the amount of time it takes for the system to reach its final barotropic state, by time stepping Eq. (19) forward in time while holding the lower-boundary PV fixed. For a stratosphere with a depth of around 32 km ($z_{\text{top}} = 4$ for a scale height of $H_s = 8$ km), assuming $\gamma = 0.02$ and a Coriolis parameter akin to that at 10° latitude, it takes around 3 years for the system to become barotropic.

This long relaxation time makes it unlikely that the barotropic state is ever reached in the real stratosphere, since unsteady processes can disrupt the simple state assumed in this model. For instance, tropospheric thermal forcing does not remain steady on the order of years, as there is a seasonal cycle in heating. Furthermore, since the β effect is not included in this simple framework, we ignore the possibility of the excitation of large-scale waves (and their corresponding effects) as a part of the response to tropospheric thermal forcing.

Indeed, the vertical propagation of planetary waves into the stratosphere has been cited as one potential reason for the observed anticorrelation between tropospheric and lower-stratospheric temperature (Dima and Wallace 2007; Grise and Thompson 2013). Here, we offer an alternative perspective, by returning to the schematic shown in Fig. 1. In the case that there is constant Coriolis force everywhere, there would be no stationary Rossby wave associated with tropospheric heating. But, at least according to the proposed theory, a cold anomaly (that is not related to convective overshooting) would still form above the tropopause. Of course, in the real world, β allows for a steady wave response (Gill 1980) that could disrupt the simple atmospheric state we have proposed. In this case, the quasi-balanced response of the stratosphere could occur in tandem with the vertical propagation of planetary waves (which are excited as part of the tropospheric thermal forcing), though a thorough investigation of this is left to future work.

In light of this, the intermediate states between the fast stratospheric response (ϕ_b in Fig. 2) in which the anomaly decays exponentially with height, and the barotropic steady-state response in which the boundary anomaly is communicated throughout the depth of the stratosphere (ϕ in Fig. 2), could be important. For practical purposes, the geopotential anomaly is not as important as the associated radiative heating, which is potentially important for tracer transport into the stratosphere. Figure 3 shows the nondimensional diabatic heating profiles with height after 30 days of integration, for a stratosphere subject to an imposed tropopause geopotential anomaly that is associated with a unitary nondimensional anticyclonic PV, under varying magnitudes of stratospheric radiative relaxation rates. The diabatic heating profiles are normalized by the radiative relaxation rate. For comparison purposes, we show the temperature anomaly associated with the (time-independent) zero perturbation PV geopotential solution (i.e., an infinite radiative-relaxation time scale), even though there is no associated diabatic heating, by definition. Figure 3 shows that after 30 days, there is nontrivial lifting (in height) of the diabatic heating anomaly over time. The stronger the strength of radiative relaxation, the faster the diabatic heating anomaly is communicated into the stratosphere.

These calculations show that tropospheric heating imposes a positive tropopause geopotential anomaly, which elicits a quasi-balanced response in the stratosphere. The fast stratospheric response is simply an anomaly that decays in the vertical according to the Rossby penetration depth. On slower time scales, radiative relaxation induces an upward migration of the anomaly. The radiative relaxation rate, the horizontal scale of the anomaly, and the Coriolis parameter all determine the upward migration rate, as shown in Haynes et al. (1991). Thus, the ensuing, time-dependent temperature response in the stratosphere is also tied to these parameters. In the next section, we will elaborate on the ideas put forth in this conceptual model in a zonally symmetric framework, and analyze, in detail, the sensitivity of the stratospheric response to tropospheric forcing, with regards to these parameters.

3. Troposphere–stratosphere response to SST

In the previous section, we used a simple QGPV framework to understand how an SST anomaly can impose a tropopause geopotential anomaly and therefore elicit a quasi-balanced response in the stratosphere. However, we used the tropopause as a lower boundary condition for the stratosphere when in reality, the tropopause and stratosphere are coupled. In this section, we develop a simple, zonally symmetric, coupled troposphere–stratosphere model, and explore how radiation and wave drag can modulate the response of the stratosphere to SST forcing.

a. Model formulation

Lin and Emanuel (2022) formulated a linear, coupled troposphere–stratosphere model, but in the context of unsteady equatorial waves. In that linear system, a convecting, quasi-equilibrium troposphere was coupled to a dry and passive stratosphere. We use the same nondimensional system derived in Lin and Emanuel (2022), except we only consider steady, zonally symmetric circulations. The tropospheric system is governed by

$$yv_0 - F(u_0 + u_1) = 0, \tag{21}$$

$$-\frac{\partial \phi_0}{\partial y} - yu_0 = 0, \tag{22}$$

$$yv_1 - F(u_0 + u_1) - D_t u_1 = 0, \tag{23}$$

$$yu_1 = \frac{ds^*}{dy}, \tag{24}$$

$$\frac{\partial v_0}{\partial y} + \frac{\partial v_1}{\partial y} + \frac{\partial \omega}{\partial y} = 0, \tag{25}$$

where u_0 and v_0 are the barotropic zonal and meridional winds (constant with height), u_1 and v_1 are the baroclinic zonal and meridional winds, ϕ_0 is the barotropic geopotential, s^* is the saturation moist entropy (that is assumed to be vertically constant, as in a quasi-equilibrium troposphere), D_t is a nondimensional Rayleigh damping coefficient, and

$$F = \frac{aC_d|\overline{\mathbf{V}}|}{\beta L_y^2 h_b} \tag{26}$$

is a nondimensional surface friction coefficient (derived in Lin and Emanuel 2022), where C_d is the drag coefficient, h_b is the boundary layer depth, L_y is the meridional length scale, β is the meridional gradient of the Coriolis force, a is the radius of Earth, and $\overline{\mathbf{V}}$ is the basic-state surface wind speed magnitude. The vertical structure of the baroclinic variables are determined by V_1 [Eq. (5)]. Note that while there are equations for the tropospheric thermodynamics in Lin and Emanuel (2022), they are omitted here. Since s^* is taken to be specified, representative of an SST forcing, there are six unknown variables, (u_0, u_1, v_0, v_1, ω, ϕ_0) and five equations. The system will be completed with a formulation of boundary conditions that will couple the troposphere system to a stratosphere (and provide the last equation).

In the ensuing text, terms with an overlying hat are dimensional. $\hat{D}_t$, the (dimensional) inverse time scale of the Rayleigh damping coefficient is

$$\hat{D}_t \rightarrow \frac{\beta L_y^2}{a} D_t. \tag{27}$$

In Eq. (23), $D_t u_1$ acts as a relaxational wave drag on the zonal flow. It does not act on the coupling between the troposphere and stratosphere, and is only used to diagnose v_1 (which by definition, has a value of zero at the tropopause). Thus, D_t modulates the baroclinic vertical velocity profile in the zonally symmetric meridional overturning circulation.

As formulated, the tropospheric system represents an atmosphere in which temperature anomalies in the vertical are restricted to follow the moist adiabat. The associated baroclinic mode, which is forced through surface enthalpy fluxes (s^*), can then excite the barotropic mode through surface friction (Lin and Emanuel 2022). The barotropic mode then excites the stratosphere. However, the stratospheric circulation becomes uncoupled with the tropospheric circulation when $F = 0$ in this case, the tropospheric solution simply obeys Eqs. (23)–(25), and the barotropic mode (as well as the stratospheric state to tropospheric forcing) becomes ill-defined. This implies that friction has an outsized influence on stratospheric circulations. However, this may not be true in reality, since the barotropic mode can also be coupled to the baroclinic mode through nonlinearity and vertical wind shear. Both of these processes are not represented in this work.

The stratosphere is formulated in log-pressure coordinates and assumed to be in hydrostatic balance (see chapter 3 of Andrews et al. 1987). The steady, linear, zonally symmetric, nondimensional equations of the stratosphere are also derived from the system used in Lin and Emanuel (2022), and summarized below:

$$yv_s - D_s u_s = 0, \tag{28}$$

$$-\frac{\partial \phi_s}{\partial y} - yu_s = 0, \tag{29}$$

$$\frac{\partial v_s}{\partial y} + \frac{1}{\rho_s}\frac{\partial(\rho_s w_s)}{\partial z^*} = 0, \tag{30}$$

$$w_s S = -\alpha_{\text{rad}}\frac{\partial \phi_s}{\partial z}, \tag{31}$$

$$\rho_s = \exp\left[\frac{H}{H_{s,s}}(1 - z^*)\right], \tag{32}$$

where subscripts denote quantities in the stratosphere, w_s is the log-pressure vertical velocity, S is a nondimensional stratospheric stratification, ρ_s is the basic-state density, H is the dimensional tropopause height, $H_{s,s}$ is the dimensional-scale height in the stratosphere, the log-pressure vertical coordinate $z^* \equiv -H\ln(p/p_t) + 1$ is defined such that $z^* = 1$ is the

bottom boundary, or the tropopause, and $\alpha_{\rm rad}$ is the nondimensional radiative damping time scale in the stratosphere:

$$\hat{\alpha}_{\rm rad} \rightarrow \frac{\beta L_y^2}{a}\alpha_{\rm rad}. \tag{33}$$

Relaxational wave drag, $D_s u_s$, is included only in the zonal momentum equations, as similarly used by PE99. It is not necessary that $D_s = D_t$, though discontinuities in the meridional velocity at the tropopause will occur if $D_s \neq D_t$. This form of wave drag is simplistic, and it is a rather poor representation of the response of the circulation to external forces (Ming et al. 2016b).

Finally, S plays an important role in the behavior of this model, and is

$$S = \frac{N^2 H^2}{\beta^2 L_y^4}, \tag{34}$$

where N is the buoyancy frequency. Note, there is no explicitly imposed thermal or mechanical forcing in the stratosphere. Thus, we consider a stratosphere entirely forced from the troposphere.

b. Stratospheric response to tropopause forcing

In the case of an isolated stratosphere subject to a tropopause forcing, the stratospheric equations can be reduced to a single differential equation for the geopotential:

$$\frac{\partial^2\phi}{\partial z^2} - \frac{H}{H_{s,s}}\frac{\partial\phi}{\partial z} + \frac{\xi}{y^2}\left[\frac{\partial^2\phi}{\partial y^2} - \frac{2}{y}\frac{\partial\phi}{\partial y}\right] = 0, \tag{35}$$

where

$$\xi = \frac{D_s S}{\alpha_{\rm rad}} = \frac{\hat{D}_s}{\hat{\alpha}_{\rm rad}}\frac{N^2 H^2}{\beta^2 L_y^4} \tag{36}$$

is a nondimensional term that depends on the ratio between the time scale of wave drag to that of radiation. This quantity is equivalent to a "dynamical aspect ratio" that describes the ratio of the vertical to horizontal scale of the circulation response to an imposed forcing (Garcia 1987; PE99; Haynes 2005; Ming et al. 2016b). As detailed in Ming et al. (2016b), who incorporated an additional external heating in the stratosphere, when the aspect ratio is large ($\xi \gg 1$), the external heating is narrow and primarily balanced by upwelling, and when the aspect ratio is small ($\xi \ll 1$), the external heating is broad and primarily balanced by Newtonian cooling. In this study, the interpretation of ξ does not have exactly the same meaning, since we do not impose a temperature-independent external heating to the system (which in the real world would arise from absorption of radiation by ozone)—our simple system is instead forced via the tropopause geopotential, and upwelling always balances Newtonian cooling. Here, ξ better describes the geopotential response with height. As we shall see later, when the radiative time scale is much faster than the wave drag time scale ($\xi \ll 1$), the meridional derivative terms are small and the system will become nearly barotropic in the vertical. On the other hand, when the wave drag time scale is much faster than the radiative time scale ($\xi \gg 1$), the stratospheric signature of the tropopause anomaly is muted. Note the presence of L_y, which indicates the importance of the horizontal scale of the anomaly.

Equation (35) can be solved numerically, discretizing the grid in the meridional and vertical directions. The stratospheric geopotential is also subject to a zero temperature anomaly at the top of the domain, or equivalently, zero derivative of the geopotential. The geopotential anomaly is enforced to be zero on the northern and southern borders. For illustrative purposes, we first solve the equations under a fixed lower boundary condition:

$$\phi(z^* = 1) = \phi_T, \tag{37}$$

where

$$\phi_T = \int_y y\exp[-4(y-2)^2] - y\exp[-4(y+2)^2]. \tag{38}$$

This represents a flat positive geopotential anomaly in the tropics (tropical heating) that decays to zero in the subtropics. As will become clear later when the solutions are coupled to the troposphere, this geopotential structure is associated with subtropical jets at $y = \pm 2$.

Figure 4 shows the stratospheric response to a tropopause geopotential anomaly, under varying values of ξ. Here, the numerical calculations confirm the mathematical analysis. Indeed, for $\xi = 0.01$ (i.e., when wave drag is very weak), radiation acts to create a nearly barotropic stratosphere, in which motion is confined to constant angular momentum surfaces. The vertical structure of the vertical velocity in this case is qualitatively similar to the thermally forced vertical mode calculated in PE99 (see their Fig. 11). When the time scale of wave drag is faster than radiation ($\xi = 100$), the vertical penetration of the tropopause geopotential anomaly is significantly muted. In fact, the vertical velocity anomalies only extend on the order of a few kilometers into the stratosphere. In this sense, the relaxational wave drag acts to both mute the vertical scale of the tropopause geopotential anomaly, and sustain a meridional overturning circulation.

As elaborated on earlier, there is much existing theoretical work that shows the response of the stratosphere to an external forcing is dependent on the strength of wave drag, the strength of radiative relaxation, and the aspect ratio of the tropopause anomaly (Garcia 1987; Haynes et al. 1991; Ming et al. 2016b). This work is mathematically similar to and agrees with the aforementioned studies. Unlike the others, this work emphasizes the role of tropopause forcing on the stratosphere, and introduces the idea that there is a quasi-balanced response in the stratosphere to tropopause forcing, via tropospheric heating.

c. Tropospheric forcing of stratospheric upwelling

Next, we couple the stratospheric equations to the zonally symmetric tropospheric equations, to show how tropospheric thermal forcing can influence stratospheric upwelling. To couple the troposphere and stratosphere, we use classical

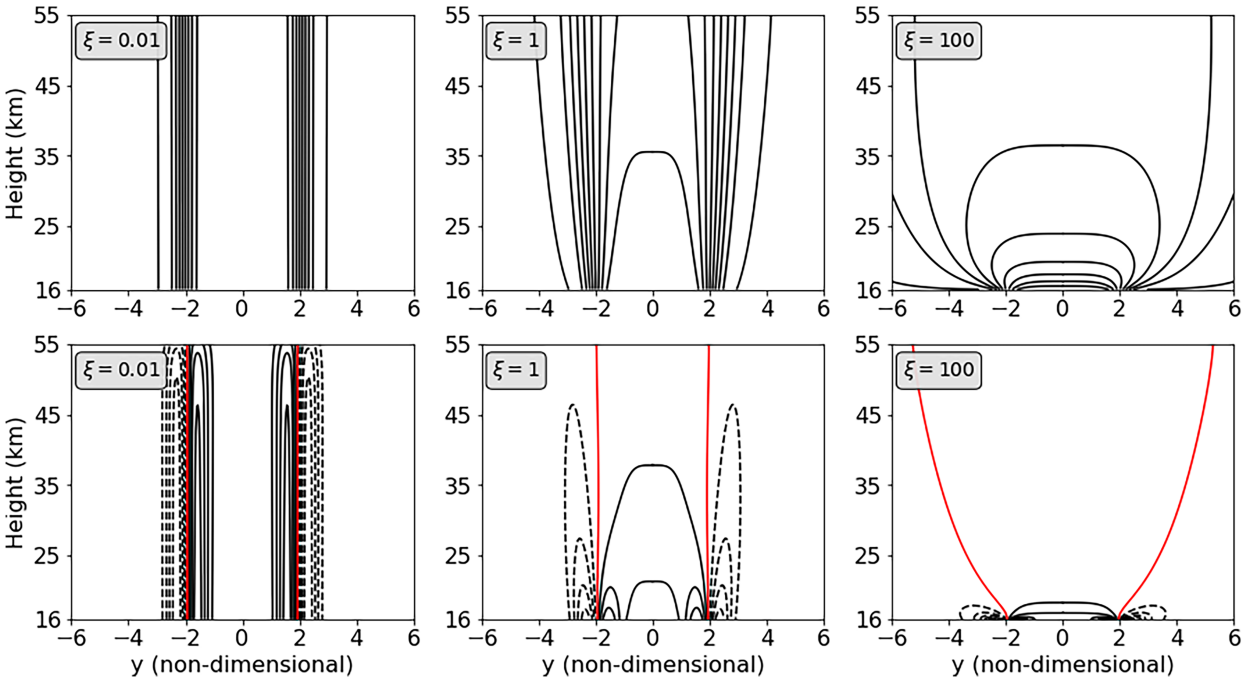

FIG. 4. (top) The zonally symmetric geopotential response to an imposed tropopause geopotential anomaly, as shown in Eq. (38), for varying values of ξ. (bottom) As in the top row, but for the zonally symmetric vertical velocity response. The red line is the zero vertical velocity isoline. Tropopause height is 16 km, and stratospheric-scale height is 8 km.

matching conditions: 1) continuity of pressure (geopotential) and 2) vertical velocity at the tropopause:

$$\phi_s(z^* = 1) = \phi_T, \tag{39}$$

$$B\omega(\hat{p}_T) = -w_s(z^* = 1), \tag{40}$$

where $B - (H_{s,t}/H)[(p_s - p_t)/p_t]$ is a scaling coefficient between pressure velocity and vertical velocity (Lin and Emanuel 2022). Here, p_s is the surface pressure, p_t is the tropopause pressure, and $H_{s,t}$ is the scale height of the troposphere. Solving for v_0 using Eqs. (25), (39), and (40), and assuming zero flow at the boundaries, yields

$$v_0 = \frac{\alpha_{\text{rad}}}{SB}\int_y \left.\frac{\partial \phi_s}{\partial z^*}\right|_{z^*=1} dy. \tag{41}$$

Here we see that under a rigid lid condition, where $S \to \infty$, $v_0 = 0$. In addition, B is proportional to the troposphere-scale height, which itself is inversely proportional to the dry stratification of the troposphere. Hence, SB can also be thought of as a scaled ratio of the troposphere buoyancy frequency to the stratosphere buoyancy frequency. The strength of radiative relaxation also appears in the numerator. This is because the magnitude of the tropospheric barotropic mode is determined, in part, by stratospheric dynamics.

Equations (21) and (24) are used to solve for u_0 in terms of the stratosphere and the external forcing:

$$u_0 = y\frac{1}{\xi\gamma}\int_y \left.\frac{\partial \phi_s}{\partial z^*}\right|_{z^*=1} dy - \frac{1}{y}\frac{ds^*}{dy}, \tag{42}$$

where

$$\gamma = \frac{FB}{D_S} \tag{43}$$

is an additional nondimensional parameter that qualitatively represents the ratio between stratospheric and tropospheric drag (there is tropospheric wave drag, but it does not act on the barotropic mode, only on the baroclinic mode). γ is not entirely independent from ξ, since D_s appears in both. Again, under the rigid lid condition, $\xi \to \infty$, such that the barotropic zonal wind becomes only a function of the tropospheric forcing. Note again that when $F = 0$, the barotropic mode becomes ill-defined, since it is no longer coupled to the baroclinic mode.

In order for the continuity of pressure to be satisfied, the geopotential at the lower boundary of the stratosphere must satisfy Eqs. (6) and (39). Combining Eqs. (6), (22), (39), and (42) yields

$$\left.\frac{\partial \phi_s}{\partial y}\right|_{z^*=1} - y^2\frac{1}{\xi\gamma}\int_y \left.\left(\frac{\partial \phi_s}{\partial z}\right)\right|_{z^*=1} dy = [1 - V_1(\hat{p}_t)]\frac{ds^*}{dy}, \tag{44}$$

which is an equation for the boundary geopotential entirely in terms of the external forcing, s^*. The Rayleigh damping coefficient for stratospheric wave drag does not appear in the boundary condition, since

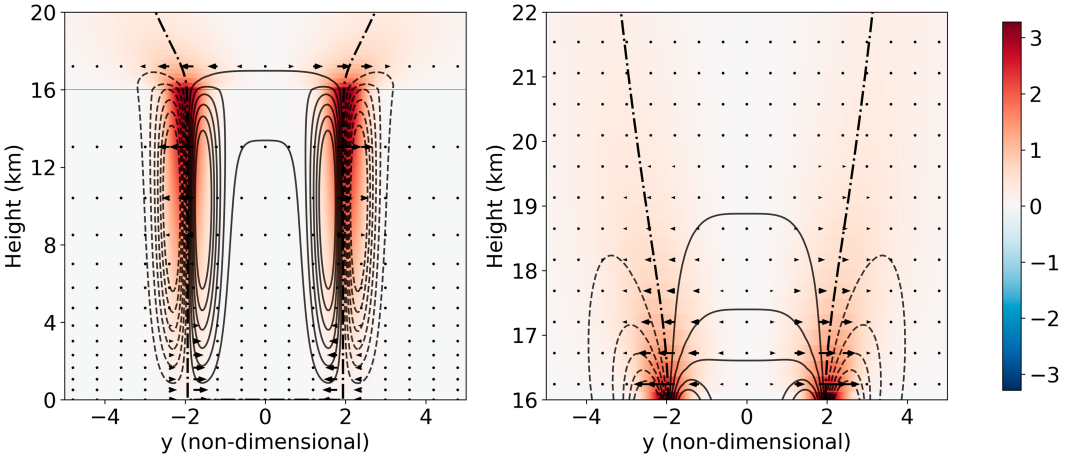

FIG. 5. (left) The zonally symmetric response to an SST (s^*) forcing shown in Eq. (47). Zonal winds are shown in colors (red for westerlies), contours show vertical motion (w), with contour spacing of 0.005, starting at 0.03. Dot–dashed line is the zero w isoline, and arrows show the meridional motion. The tropopause is shown by the thin gray line. "Earthlike" parameters of $\xi = 150$, $\gamma = 30$ are used. (right) As in the left panel, but zoomed in on the stratosphere. Contour spacing is 0.002, starting at 0.01.

$$\frac{1}{\xi\gamma} = \frac{\alpha_{\text{rad}}}{D_s S}\frac{D_s}{FB} = \frac{\alpha_{\text{rad}}}{SFB}. \tag{45}$$

When $\xi\gamma$ is large, the boundary condition simply reduces to Eq. (6), with $\phi_b = 0$. When $\xi\gamma$ is small, s^* becomes a multiple of a double integral in y of the vertical derivative of the stratospheric geopotential at the tropopause.

Incorporating Eq. (44) as the lower boundary condition is numerically tricky given the meridional integral, since it precludes the inversion of a sparse matrix. The integral can be removed by dividing by y^2 and differentiating with respect to y, which yields

$$\frac{-2}{y^3}\frac{\partial\phi_s}{\partial y} + \frac{1}{y^2}\frac{\partial^2\phi_s}{\partial y^2} - \frac{1}{\xi\gamma}\frac{\partial\phi_s}{\partial z} = [1 - V_1(\hat{p}_t)]\left(\frac{1}{y^2}\frac{d^2s^*}{dy^2} - \frac{2}{y^3}\frac{ds^*}{dy}\right), \tag{46}$$

where the entire equation is evaluated at $z^* = 1$. This boundary condition leads to a sparse matrix that can be easily incorporated into a numerical solver.

Before continuing with the numerical solutions, we formulate the SST forcing in the troposphere. We observe from Eq. (24) that

$$s^* = \int y u_1 \, dy \tag{47}$$

such that we can specify the baroclinic wind response to obtain a suitable s^* anomaly. Here, we specify

$$u_1(y) = -\exp[-4(y-2)^2] - \exp[-4(y+2)^2], \tag{48}$$

which is akin to subtropical jets symmetric about the equator. Note, the meridional baroclinic wind is

$$v_1 = \frac{F}{y}u_0 + \frac{D_t + F}{y^2}\frac{ds^*}{dy}. \tag{49}$$

Numerical evaluation of v_1 requires that the meridional derivative of s^* go to zero faster than y^2 in the limit of $y \to 0$; otherwise, v_1 will become unstable for small values of y on the numerical grid. However, the stratospheric solution does not depend on v_1, so this constraint merely ensures a smoothly varying tropospheric circulation. Thus, $u_1(y)$ is chosen to satisfy this constraint. We proceed by numerically solving the stratospheric system [Eq. (35)] with the modified boundary condition shown in Eq. (46), as well as the s^* forcing shown in Eq. (47). See the appendix for more details on the numerical solver.

To set the nondimensional parameters of the model, we use Earthlike parameters of $N^2 = 6 \times 10^{-4}$ s^{-2}, $H = 16$ km, $H_{s,t} = H_{s,s} = 8$ km, $\beta = 2.3 \times 10^{-11}$ s^{-1} m^{-1}, $L_y = 1200$ km (such that $y = 1$ represents approximately 10° of latitude), $C_d = 10^{-3}$, and $|\mathbf{V}| = 3$ m s^{-1}. Furthermore, we choose $T_b = 303$ K, a surface pressure of 1000 hPa, and a tropopause pressure of 100 hPa. The vertical temperature profile in the troposphere follows a pseudoadiabatic lapse rate (neglecting changes to heat capacity; see Eq. 4.7.5 of Emanuel 1994), such that $[\overline{T}] \approx 264.5$ K and $\overline{T}(p_t) \approx 176.1$ K. With these values, $V_1(p_t) \approx -2.3$.

Since α_{rad} and $\hat{D}_t$ play critical roles in the stratospheric response to an imposed tropopause geopotential anomaly, we will explore the nondimensional space of ξ and γ. Still, it is helpful to note the estimates of the general order of magnitudes of these quantities in the real stratosphere. Hitchcock et al. (2010) estimated the radiative relaxation time scale to be approximately 25 days in the lower tropical stratosphere. The magnitude of the Eliassen–Palm (EP) flux divergence is around $O(1)$ m s^{-1} day^{-1} in the subtropics, but decays rapidly as one moves equatorward into the deep tropics (Randel et al.

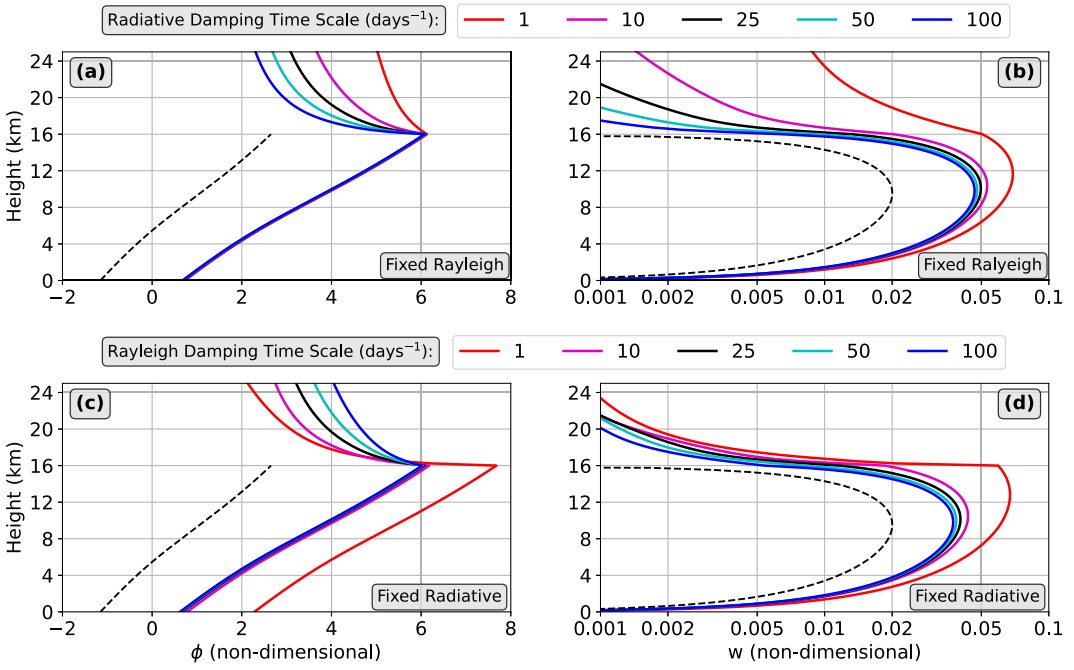

FIG. 6. (a) Vertical profiles of nondimensional geopotential and (b) vertical velocity, at $y = 1.5$, for varying values of radiative relaxation, at a fixed Rayleigh damping (wave drag) of (25 days)$^{-1}$. Dashed lines show the geopotential and vertical velocity associated with a pure baroclinic mode (normalized so that the peak vertical velocity is 0.02). (c),(d) As in (a) and (b), respectively, but for varying values of stratospheric Rayleigh damping, at a fixed radiative relaxation rate of (25 days)$^{-1}$. Tropopause is defined at 16 km, and tropospheric Rayleigh damping is fixed at (25 days)$^{-1}$.

2008). For a perturbation zonal wind speed of $O(10)$ m s^{-1}, this corresponds to a Rayleigh damping rate of around 10 days^{-1} and slower.

For now, we restrict the analysis to "Earthlike" parameters, with $\hat{\alpha}_{\rm rad} = 25\,{\rm days}^{-1}$, and $\hat{D}_s = \hat{D}_t = 25\,{\rm days}^{-1}$. This choice leads to $\xi \approx 150$ and $\gamma \approx 30$. Thus, $\xi\gamma$ is large, and the tropopause geopotential can be approximated as simply a multiple of s^*. Figure 5 shows the zonally symmetric, linear response to the prescribed, equatorially symmetric SST forcing. We observe a meridionally shallow, thermally direct overturning circulation in the troposphere, associated with subtropical jets at $|y| = 2$ that decay exponentially with height into the stratosphere. The tropopause geopotential is elevated in the tropical region ($|y| < 2$) (not shown). Associated with this elevated tropopause geopotential is a weak, meridionally shallow, thermally indirect overturning circulation in the stratosphere, with upwelling around an order of magnitude smaller than peak upwelling in the troposphere. Note that the tropospheric thermally direct overturning circulation in this model is not meant to realistically mimic the Hadley circulation, since linear models do not capture the dynamics of the Hadley circulation (Held and Hou 1980). Rather, its purpose in this model is to understand how tropopause geopotential anomalies associated with tropospheric circulations influence the stratospheric circulation.

What is the sensitivity of the stratospheric circulation to $\hat{\alpha}_{\rm rad}$? Figures 6a and 6b show the vertical profile of anomalous geopotential and vertical velocity, for varying values of $\hat{\alpha}_{\rm rad}$. In all the solutions presented here, the tropospheric wave drag is fixed. We first observe that for all the solutions, the geopotential anomaly maximizes at the tropopause, and there is a significant barotropic geopotential component associated with all of the solutions. These positive geopotential anomalies decay as one moves upward into the stratosphere, but the rate at which they decay is determined by the aforementioned parameters. When $\hat{\alpha}_{\rm rad} = (1\,{\rm day})^{-1}$, we observe a slow decay of the tropopause geopotential as one moves upward into the stratosphere, and large upwelling values in the lower stratosphere. In contrast, when radiation is very slow [$\hat{\alpha}_{\rm rad} = (100\,{\rm days})^{-1}$], there is almost no penetration of the tropospheric vertical velocity into the stratosphere. This is associated with a tropospheric vertical velocity profile that is nearly entirely composed of the first baroclinic mode. As expected, radiative damping plays a large role in the communication of the tropopause forcing into the stratosphere.

The stratospheric response to a steady tropopause geopotential anomaly also shows a strong dependence to $\hat{D}_s$. This is not surprising, given the criticality of wave drag in the zonally symmetric solutions. Figures 6c and 6d show the solutions with varying $\hat{D}_s$ and a fixed radiative damping time scale. The behavior of the coupled solutions are qualitatively similar to that inferred from the isolated stratosphere solutions, in that faster wave drag time scales increase the decay of the tropopause geopotential into the stratosphere. In addition, faster wave drag time scales are associated with increased upwelling

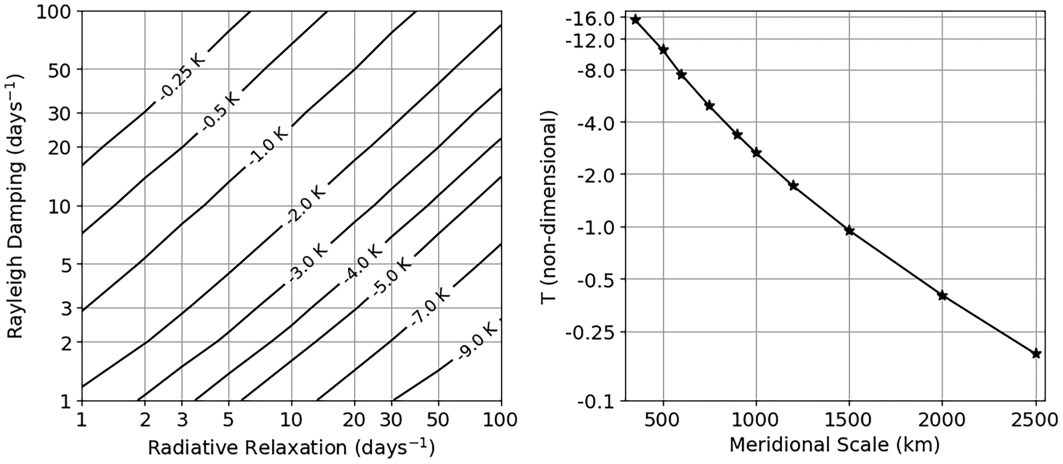

FIG. 7. (left) Temperature anomaly right above the tropopause, per degree of warming in the boundary layer, as a function of the radiative relaxation and Rayleigh damping (wave drag) time scales. Rayleigh damping time scale is fixed in the troposphere and varied in the stratosphere. Both the abscissa and ordinate axes are in log coordinates. (right) Temperature anomaly right above the tropopause, per degree of warming in the boundary layer, as a function of the meridional length scale, L_y (km), for fixed Rayleigh damping and radiative relaxation. Ordinate axis is logarithmic.

in the lower stratosphere, though the differences across the parameters shown are smaller in magnitude than that when varying the radiative damping time scale. This result could be a result of the simple relaxational form of wave drag used in this study, which does not capture detailed aspects of wave forcing (Ming et al. 2016b). Regardless, the numerical solutions confirm the mathematical analysis, in that both radiative damping and wave drag can modulate the stratospheric response to tropospheric forcing. Note, in a similar linear system, PE99 found solutions to a stratosphere perturbed through tropospheric thermal forcing that showed stratospheric upwelling nearly comparable in magnitude to that of the troposphere, which was deemed as unrealistic. In PE99, the radiative relaxation time scale was $(10\ \text{days})^{-1}$ and the relaxational wave drag time scale was $(500\ \text{days})^{-1}$, which corresponds to small ξ, and large penetration of the tropospheric circulation into the stratosphere.

The vertical shape of the geopotential profiles above the tropopause also allows for an estimate of the magnitude of the tropopause temperature cold anomaly as a function of tropospheric heating. Figure 7, left, shows the temperature anomaly right above the tropopause, per degree of warming in the boundary layer, as a function of the radiative damping and Rayleigh damping time scales. In general, the longer the radiative damping time scales, the larger the temperature anomaly (as pointed out by Randel et al. 2002). In addition, there is also a strong dependence of the tropopause temperature anomaly on the Rayleigh damping time scale: the faster the damping, the larger the magnitude of the temperature anomaly. It is clear that both the magnitudes of the Rayleigh damping (wave drag) and radiative damping play significant roles in modulating the temperature anomaly above the tropopause.

Interestingly, for "Earthlike" estimates of the time scale of Rayleigh damping and radiative relaxation $[O(10\ \text{days})^{-1}]$, the temperature anomalies just above the tropopause are around 2–3 times the magnitude of the boundary layer anomalies, slightly larger than what is observed in convecting regions of the tropical atmosphere (see Fig. 5a in Holloway and Neelin 2007). This theory thus provides a scaling argument for the degree of tropopause cooling that is expected per degree of boundary layer warming. Note that the derivative of the geopotential is discontinuous across the tropopause in this model, since we assume an instantaneous transition between quasi-equilibrium thermodynamics in the troposphere, and dry, passive dynamics in the stratosphere.

These theoretical results provide a potential explanation for the observed correlation between tropical-averaged SST anomalies and tropical stratospheric upwelling (Lin et al. 2015), as well as the anticorrelation between SST and tropopause temperature (Holloway and Neelin 2007). First, an SST anomaly is communicated throughout the depth of the troposphere through moist convection. Indeed, observations have found strong positive correlations between the tropopause geopotential anomaly and the boundary layer temperature anomaly (Holloway and Neelin 2007). The tropopause geopotential anomaly is initially associated with cold temperature anomalies just above the tropopause. The strength of radiative relaxation then determines the time scale at which the geopotential anomaly rises in the stratosphere through diabatic heating. In the zonally symmetric case, the presence of wave drag, through conservation of angular momentum, disrupts this process and induces a meridional overturning circulation that mediates the vertical scale at which the geopotential anomaly can rise in the stratosphere.

Our work shows that, at least in the zonally symmetric case, the ratio between the strength of radiative relaxation and that of Rayleigh damping are significant factors in determining the response of the stratosphere to an SST anomaly. However,

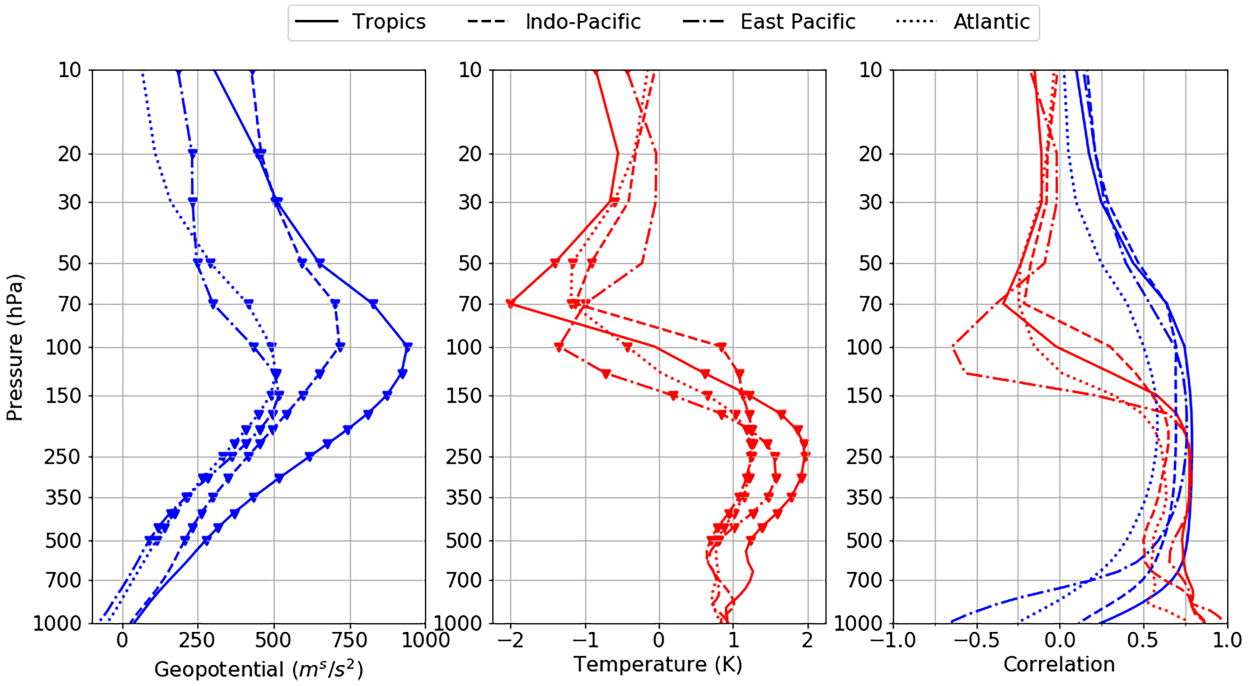

FIG. 8. (left) Linear coefficient of geopotential at varying levels, regressed onto regionally averaged SST anomaly. Above 500 hPa, significant correlations at the 1% level (two sided) are denoted by upside-down triangles. (center) As in the left, but for temperature. (right) Vertical dependence of the correlation coefficients for geopotential (blue) and temperature (red). The regions are the entire tropics (20°S–20°N;solid), the Indo-Pacific region (40°–120°E;dashed), the east Pacific region (180°–260°E; dot–dashed), and the Atlantic region (80°–0°E; dotted). Vertical level is scaled as the logarithm of pressure.

there are a number of other quantities unveiled through the nondimensionalization that are also important. Surface friction, for instance, factors into γ. In general, increasing the magnitude of F does little to change the behavior of the stratospheric response to tropospheric forcing when ξ is large, since F only enters in γ and $\xi\gamma$ is what matters for the tropopause boundary condition. The tropospheric and stratospheric stratification, as well as the shape and length scale of the SST (or tropopause) perturbation (L_y), also factor into the nondimensional parameters that control the vertical decay scale of tropopause geopotential anomalies. The horizontal scale of the SST anomaly can also be quite important, due to the dependence of S on L_y^{-4}. Figure 7, right, shows the dependence of the temperature anomaly above the tropopause on L_y. There is an approximately logarithmic scaling of the temperature anomaly with the meridional length scale of the tropopause anomaly, at least across the range of L_y in the experiments. Correspondingly, the geopotential response in the stratosphere is muted for small L_y (not shown). Thus, large horizontal-scale tropospheric heating anomalies have a larger penetrative depth into the stratosphere, but are also associated with smaller (in magnitude) temperature anomalies at the tropopause.

4. Tropopause forcing in reanalysis data

In this section, we evaluate the proposed theory using the ERA5 (Hersbach et al. 2019b,a). We use monthly fields of SST, geopotential, and temperature, over the years 1979–2022. The quasi-biennial oscillation (QBO) is regressed out of the geopotential and temperature fields, by using the 50-hPa zonal wind averaged over the tropics. In particular, we will analyze correlations between metrics of tropospheric warming and stratospheric cooling, on the global scale and the local scale.

To begin, we regress the anomalous tropical-averaged geopotential, at different vertical levels, onto the tropical-averaged SST anomaly. Anomalies are generated by subtracting the linear trend in each field, as well as the seasonal cycle. Figure 8, solid lines, shows the coefficients of the linear regressions of geopotential and temperature onto SST. We first observe an approximate moist-adiabatic structure in the tropical tropospheric geopotential, consistent with quasi equilibrium and the findings of previous studies (Holloway and Neelin 2007). We also see a large, significant correlation ($r \approx 0.75$) between tropical-averaged SST and the corresponding 100-hPa geopotential. The magnitude of the geopotential anomaly maximizes at 100 hPa, which is interpreted as an approximate tropopause level, since below this level there is warming, and above this level there is cooling (this is not exact, since the cold-point tropopause could occur above this level). Note the similarity to the geopotential profile shown in Fig. 6, which also maximizes around the climatological tropopause. This is indicative of a tropopause geopotential anomaly that is induced by an SST anomaly. The coefficient magnitudes and correlations decay with increasing height in the stratosphere, but are still statistically significant and nonnegligible even at 20 hPa. Note, for a pure baroclinic mode anomaly, the surface

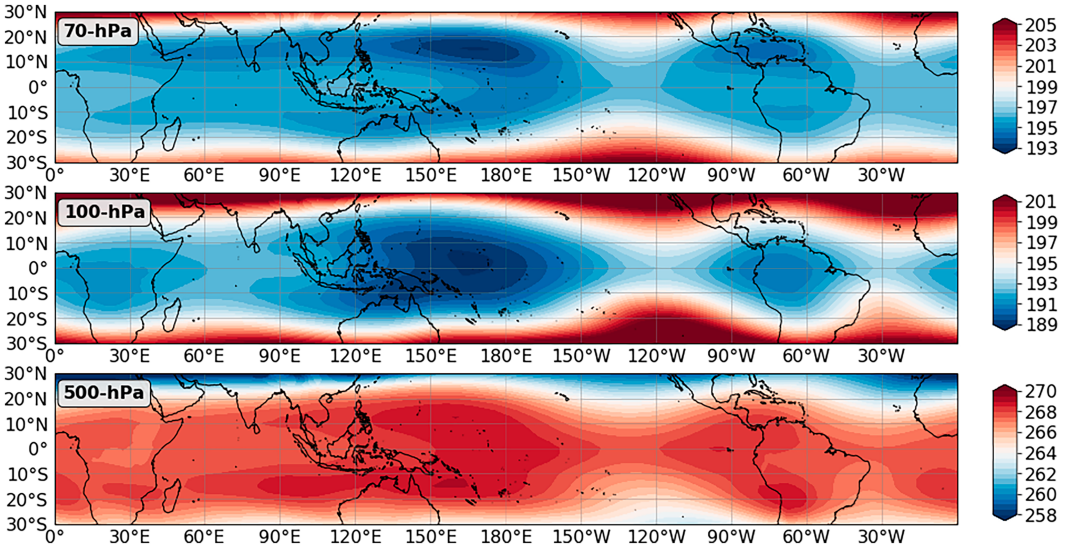

FIG. 9. DJF-averaged climatological temperature at (top) 70, (middle) 100, and (bottom) 500 hPa. Note the strong anticorrelation in troposphere and lower-stratospheric temperature.

geopotential would be anticorrelated with the upper-troposphere anomaly (and the SST). Thus, when the surface geopotential is positively correlated with the upper-tropospheric anomaly, there is a significant barotropic component to the geopotential profile. We indeed observe that the tropical-averaged surface geopotential is positively correlated with both SST and the upper-tropospheric geopotential, highlighting the role of the barotropic mode and the troposphere's communication with the stratosphere.

The temperature structure of the tropical troposphere is also approximately moist adiabatic, as also shown in Holloway and Neelin (2007). Figure 8 also shows that the tropics-averaged 70-hPa temperature is modestly but significantly anticorrelated ($r \approx -0.34$) with surface temperature. We also observe temperature anomalies at 70 hPa (lower stratosphere) to be approximately 2 times larger in magnitude than that of the surface, which is in agreement with the estimates shown in Fig. 7. This is not exactly equivalent with the quantity derived in the left portion of Fig. 7, as the regridded, pressure-interpolated output for ERA5 does not have many vertical levels near the tropopause, such that sharp reversals in the temperature response might be smoothed out. While data on the underlying model levels are available at a much higher vertical resolution, the ensuing analysis is very data intensive and left for future work.

The same relationships are also observed on regional scales (the Indo-Pacific, east Pacific, and the Atlantic), as shown in Fig. 8. The geopotential anomalies maximize at 100 hPa in the Indo-Pacific, at 125 hPa in the Atlantic, and at 150 hPa in the east Pacific. Thus, the level at which the geopotential anomaly maximizes is influenced by the mean SST of the region (the east Pacific has the coldest climatological SSTs, while the Indo-Pacific has the warmest). In addition, the cold anomaly associated with SST warming maximizes above the level of maximum geopotential. The regional-scale geopotential anomalies persist upward to around 50 hPa, though the correlations drop significantly in magnitude, and the statistical significance ceases around 50 hPa. This means that regional- and local-scale variations in the lower-stratospheric geopotential (50 and 70 hPa) are strongly influenced by the tropopause geopotential in the same region. In general, the temperature anticorrelations are strongest in the east Pacific region—this may because there are large SST perturbations in this region as a consequence of El Niño–Southern Oscillation variability, increasing the signal of the relationship.

Of course, this analysis is not definitive proof that there is a quasi-balanced response of the stratosphere to tropopause forcing. After all, if stratospheric temperature is modulated by tropical heating through changes to wave drag (Garcia and Randel 2008; Calvo et al. 2010; Lin et al. 2015), then one would also expect the geopotential to decay with height in the stratosphere, as is shown in Fig. 8. Perhaps what would serve as stronger evidence for the processes described in this study is if the spatial signature of tropospheric warming is retained in that of stratospheric cooling. If true, this implies that lower-stratospheric temperature is also influenced by "bottom-up" processes (Garfinkel et al. 2013; Fu 2013)—not just "top-down" processes.

In the tropics, the surface temperature need not always be connected to tropospheric warming, especially if the boundary layer moist static energy is lower than the saturation moist static energy of the free troposphere. This is possible since temperature gradients in the tropical atmosphere are weak, owing to the smallness of the Coriolis force, such that convecting regions more effectively modulate the free-tropospheric moist static energy (Sobel and Bretherton 2000). Thus, we use 500-hPa temperature as a proxy for local tropospheric warming.

Figure 9 shows a map of the DJF-averaged 500-hPa climatological temperature, a proxy for tropospheric heating, and the climatological temperature at 100 and 70 hPa in the lower stratosphere [these maps are well known and have been

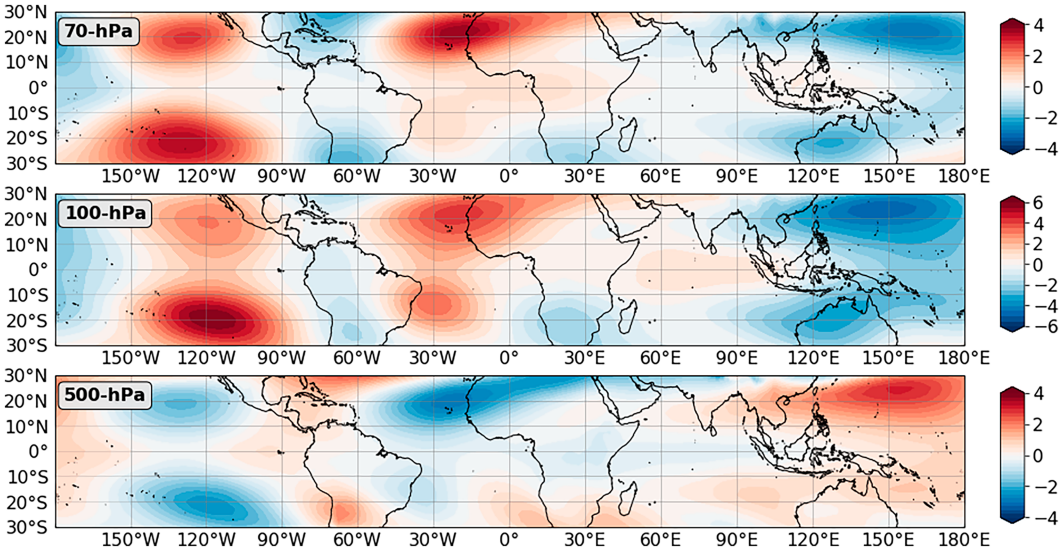

FIG. 10. DJF-averaged temperature anomaly at (top) 70, (middle) 100, and (bottom) 500 hPa. Note the strong anticorrelation in troposphere and lower-stratospheric temperature. Anomalies are calculated by subtracting the climatological monthly zonal mean, and averaging across the entire year. The color scale at 100 hPa is different than that at 70 and 500 hPa.

shown before, for instance, in Dima and Wallace (2007), Fueglistaler et al. (2009), and Grise and Thompson (2013), but with different interpretations]. Here, we observe the warmest 500-hPa temperatures are in regions typically associated with active convection (the west Pacific warm pool, equatorial South America, and equatorial Africa). Note that tropospheric heating is a by-product of convection. Furthermore, these same regions are where the coldest 100- and 70-hPa temperatures are also observed. Importantly, the coldest temperatures in the lower stratosphere occur right on or close to the equator, where the Coriolis force is small. At 70 hPa, the signature of the equatorial 100-hPa cold anomalies disappears. This may be a manifestation of the shallow vertical Rossby penetration depth of anomalies on the equator.

To further emphasize spatial variability, we compute monthly anomalies by subtracting the climatological monthly zonal mean from the climatological monthly mean, and then average these across December–February (DJF). Figure 10 shows maps of the DJF-averaged temperature anomalies at 500, 100, and 70 hPa. Note the difference in the color scale at 100 hPa. It is evident that 500-hPa temperature is an excellent predictor of both the 100- and 70-hPa temperature anomaly, though the strongest patterns are observed in the subtropical regions and associated with Rossby wave–like features. Still, spatial variability in the tropospheric temperature anomaly is remarkably retained in the spatial variability of the stratospheric temperature. Furthermore, the lower-stratospheric temperature anomalies can be rather large (upward to around 4° in magnitude at 100 and 70 hPa), though the total area encompassed by these large anomalies is small. There is also some qualitative evidence from the maps in Fig. 10 that suggests that the magnitude of the lower-stratospheric temperature anomalies is dependent on the horizontal scale of the tropospheric anomaly. For instance, from 60°W to 30°E in the Northern Hemisphere, there is a large-scale tropospheric cold anomaly of peak magnitude around 2°. The associated temperature anomaly at 100 hPa is around 4°. There is also a large-scale tropospheric warm anomaly of peak magnitude around 3° in the Asian region (90°E–180°), with 100-hPa temperature anomalies of around −6°. In contrast, smaller-scale tropospheric anomalies (10°–30°S, 150°–90°W and 45°–15°W, 10°–25°S) with comparatively weaker peak temperature anomalies are associated with 100-hPa temperature anomalies that are of similar magnitude to the 100-hPa temperature anomalies of the stronger, large-scale anomalies. This is in agreement with the proposed theory. In addition, at 70 hPa, the most prominent temperature anomalies are those associated with the large-scale tropospheric anomalies (i.e., over the northeast African and Asian regions). This is also in agreement with the theory, in that the vertical depth of the tropopause anomalies increases with the horizontal scale of the tropospheric anomaly. Of course, the analysis here is mostly qualitative, and more substantial analysis is required to further quantify the scale dependence of the lower-stratospheric temperature anomalies, which will be pursued in future work.

The remarkable correlation between tropospheric heating and stratospheric cooling can be further quantified by regressions of 500-hPa temperature against lower-stratospheric temperature, among all grid points shown in Fig. 10. Figure 11, top row, shows 2D density histograms between the 500-hPa climatological temperature and the 100-, 70-, and 50-hPa climatological temperature, as well as the linear regressions. We have subsetted the latitudinal region in this analysis to 15°S–15°N, in order to focus on the tropical regions. Per degree of warming at 500 hPa, the cooling response is around 2.0° at 100 hPa ($r = -0.84$), 0.72° at 70 hPa ($r = -0.64$), and 0.21° at

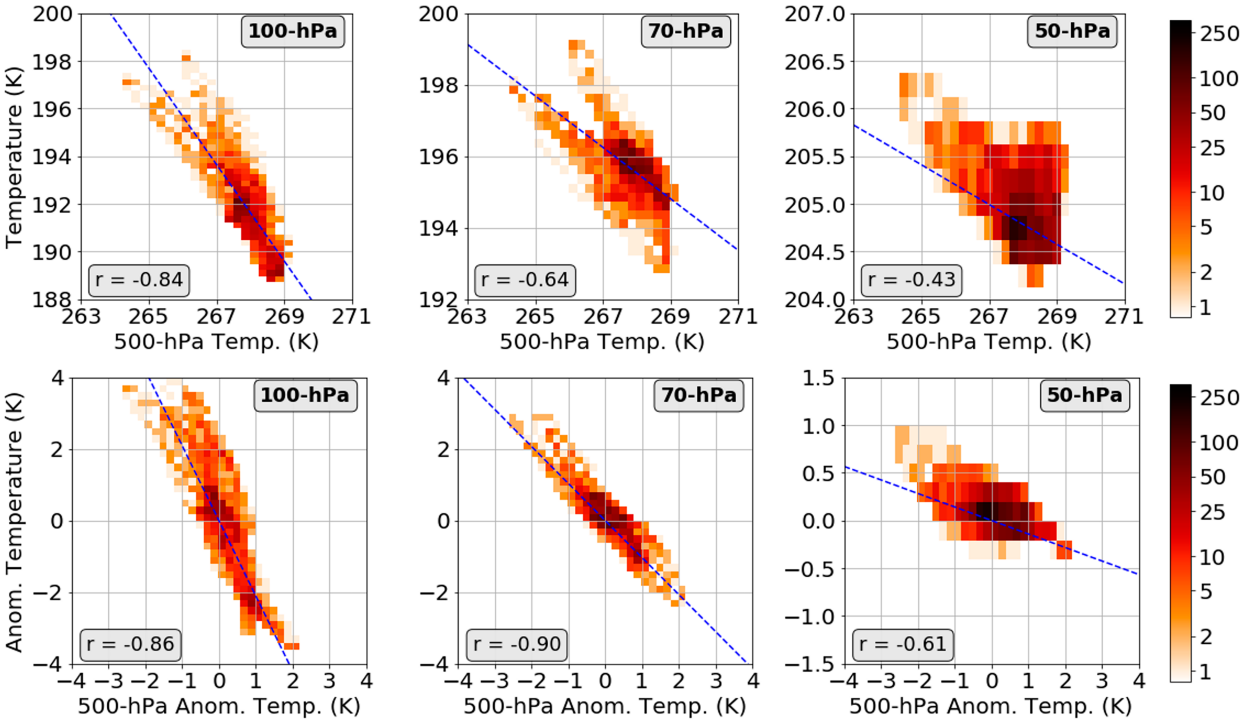

FIG. 11. (top) Gridpoint 2D histograms between the 500-hPa climatological temperature and the (left) 100-, (center) 70-, and (right) 50-hPa climatological temperature, during DJF and from 15°S to 15°N. (bottom) As in the top row, but for anomalous temperatures at each pressure level. Color scale is logarithmic, and indicates the bin count. Linear regressions are plotted as the dashed blue lines, with correlation coefficients shown on the lower left of each panel.

50 hPa ($r = -0.43$). The correlations are all significant, and generally decrease in strength as one moves up further in the stratosphere. The linear regressions of 500-hPa anomalous temperature against lower-stratospheric anomalous temperature tell a similar story, as shown in Fig. 11, bottom row. Per degree of anomalous 500-hPa temperature, there is a cooling response of around 2.1° at 100 hPa ($r = -0.86$), 1.03° at 70 hPa ($r = -0.90$), and 0.14° at 50 hPa ($r = -0.61$). Note that while this paper focuses on the tropics, the proposed mechanism need not only apply to the tropics (though Rossby wave excitation can be important outside of the tropics). In fact, the correlations are even stronger if one extends the region of analysis to 30°S–30°N.

While the monthly anomalies shown in Fig. 10 are averaged across DJF, there is significant seasonal variability in the pattern of 500-hPa tropospheric temperature (not shown). The analysis can be repeated by separating into various seasons, and we find that the local-scale anticorrelation are generally strongest during boreal winter, and weakest during boreal summer (not shown). Still, the results and interpretation remained unchanged: 500-hPa temperature is strongly anticorrelated with lower-stratospheric temperature. It is important to note that these correlations do not suggest that there are correlations on significantly smaller horizontal scales; as suggested by Fig. 10, the correlations merely reflect the large-scale structure of the temperature anomalies.

Therefore, the observational data suggest that there might be a quasi-balanced response of the stratosphere to tropospheric thermal forcing in the real world. However, there is reason to remain cautious. As detailed in section 2, separating the effect of the vertical propagation of planetary waves from that of the quasi-balanced response of the stratosphere is nearly impossible in observational data. While we restricted our analysis to 15°S–15°N, further insight into the relative contribution of each proposed mechanism to the anticorrelation between tropospheric and lower-stratospheric temperature is left for future work.

5. Summary and discussion

In this work, we present theoretical evidence for how tropopause geopotential anomalies, generated through tropospheric thermal forcing, can modulate upwelling in the stratosphere. Using a conceptual model based on the linearized QGPV equations, we show that tropospheric thermal forcing can induce a tropopause geopotential anomaly, which subsequently elicits a quasi-balanced response in the stratosphere. The tropopause anomalies initially have vertically shallow structures scaled by the Rossby penetration depth (i.e., the fast adjustment of the stratosphere). Afterward, radiative relaxation in the stratosphere acts to increase the vertical penetration of these anomalies. In the steady-state limit, where radiative equilibrium is again satisfied, the stratospheric PV becomes barotropic, though it takes on the order of years to be achieved. The solutions are akin to those of Haynes et al. (1991), who found that the stratosphere becomes barotropic above the level of forcing (in this case, the tropopause). This theory provides another

potential explanation for why cold stratospheric anomalies form above areas with local tropospheric warming. Despite the focus on the tropics in this study, this proposed mechanism need not be confined to the tropics. However, the excitation of planetary waves as a response to tropospheric heating, which was ignored for simplicity in this study, ought to be taken into account. This will be the subject of future research.

We then formulate a zonally symmetric troposphere–stratosphere linear β-plane model, which couples a convecting troposphere to a dry and passive stratosphere. We show that zonally symmetric tropospheric thermal forcing (via SST anomalies) can directly force upwelling in the lower stratosphere, provided the wave response is modeled purely as a response to the forced circulation. The stratospheric response to tropospheric forcing is controlled by two nondimensional parameters: 1) ξ, a dynamical aspect ratio (Garcia 1987; PE99; Haynes 2005; Ming et al. 2016b), and 2) γ, a ratio between the stratospheric drag and tropospheric drag. The main role of the tropospheric drag is to excite the tropospheric barotropic mode, which couples the troposphere with the stratosphere. In the limit that the radiative relaxation is much stronger than wave drag, the stratospheric response to a tropopause forcing asymptotically becomes barotropic, while in the opposite limit, the vertical length scale of the tropopause forcing becomes extremely small. We find that the stratospheric response to zonally symmetric tropospheric forcing is largely dependent on the radiative relaxation rate, the Rayleigh damping time scale of wave drag, and the horizontal scale. Our analyses show that the tropopause temperature anomaly is also modulated by all of these quantities.

We also use reanalysis data to show that tropical and regionally averaged lower-stratospheric temperatures are modestly and negatively correlated with SSTs in the same areas. In general, the temperature anomalies per degree of warming in the boundary layer are approximately equivalent to the corresponding theoretical predictions, at least when using "Earthlike" estimates of the time scale of wave drag and radiative relaxation. Furthermore, we show that the spatial variability in lower-stratospheric temperature anomalies is strongly correlated with the spatial variability in 500-hPa tropospheric temperatures. Significant correlations are seen upward to 50 hPa, which suggests that there is a quasi-balanced response of the stratospheric to tropospheric forcing. This provides a scale-dependent theory for the oft-observed anticorrelation between tropospheric warming and stratospheric cooling (Johnson and Kriete 1982; Gettelman et al. 2002; Holloway and Neelin 2007; Kim and Son 2012; Virts and Wallace 2014; Kim et al. 2018).

The widely accepted theory of tropical stratospheric upwelling is that it is mechanically driven by subtropical wave drag (Haynes and McIntyre 1987; PE99). There is ample evidence from numerical modeling suggesting that wave dissipation is a dominant mechanism that modulates mean and interannual upwelling in both the lower stratosphere and TTL (Boehm and Lee 2003; Norton 2006; Calvo et al. 2010; Ryu and Lee 2010; Gerber 2012; Ortland and Alexander 2014; Kim et al. 2016; Jucker and Gerber 2017, among many others). Of course, it is theoretically impossible to have flow across angular momentum contours without some momentum source. We emphasize that in no way does this work attempt to disprove the role subtropical wave drag has in modulating tropical stratospheric upwelling. In this model, even though wave drag acts as a Rayleigh damping, as in the linear system described in PE99, it is an important modulator of the upwelling response.

As shown in this study, the vertical penetration of the geopotential anomaly (and the rate at which the stratospheric circulation crosses angular momentum surfaces) is strongly a function of the wave drag. If the wave drag is a function of the zonal mean state, which could vary in time in part due to wave forcing (Cohen et al. 2013; Ming et al. 2016b), then the vertical penetration of the tropopause anomaly (and thus, its subsequent effect on upwelling) would also vary in time. In this view, stratospheric wave drag is, as countless studies have shown, a significant modulator of tropical upwelling. However, wave drag alone may not suffice to explain certain features of the behavior of the lower stratosphere, the foremost of which is the inverse correlation between SST and lower-stratospheric temperature anomalies, in both the zonal and meridional directions.

Our work, like PE99, investigates how tropospheric thermal forcing can modulate stratospheric upwelling. In addition to mechanical and thermal forcing, this suggests a *third* way in which the stratosphere can be forced—through the tropopause via tropospheric thermal forcing. In fact, the theoretical analysis shown in PE99 finds that in the tropics, "the existence of a thermally driven circulation and the breakdown of downward control go together" (if one accepts that what they define as viscosity is representative of large-scale drag). However, their calculation of the linear response to tropospheric thermal forcing exhibited large and unrealistic vertical penetration of the tropospheric circulation into the stratosphere. This work shows that this is likely a result of their assumptions of the strength of radiative relaxation [$\alpha_{\rm rad} = (10\ \text{days}^{-1})$] and viscosity [$\hat{D} = (500\,\text{days})^{-1}$]. With $S = O(10^2)$, this is equivalent to $\xi \approx 3$. In this regime, our theory predicts extensive penetration of the tropospheric circulation into the stratosphere, as in Figs. 4 and 6.

In general, it is difficult to infer causality from diagnostic relations. For example, in the transformed Eulerian mean equations, it is not clear how much of the wave drag is an external forcing, as opposed to a response to a circulation that has a different forcing. Of course, variations in wave drag that are independent of those of the circulation support the idea that waves can force the circulation. This aspect of the stratosphere has been well studied. But what if wave drag acted purely as a response to the circulation? (Note that these ideas are at opposite ends of the spectrum with regards to the extent waves drive the circulation.) Then, at least in our framework, the causality becomes very clear—SST forces the stratosphere by imposing a tropopause geopotential anomaly. Of course, one could take the wave drag term ($-D_s u_s$) and use it to diagnose the associated upwelling response. However, that does not imply that waves are the forcing mechanism of the circulation.

There are a few pieces of observational evidence that could be interpreted to be in favor of the proposed theory. As stated earlier, the spatial variability of lower-stratospheric temperature is strongly correlated with that of the troposphere, when considering both the climatological and anomalous temperatures. In contrast, wave drag, in its classical arguments, can only explain departures of temperature from the zonal mean (Andrews et al. 1987). This is by no means a small feat, since the annual cycle in tropical-averaged temperature near the tropopause is around 8 K, around a factor of 2 larger than the peak temperature anomalies shown in Fig. 10 (Chae and Sherwood 2007).

However, the quasi-balanced response of the stratosphere to tropopause forcing could serve as a potential explanation for a few outstanding issues. For instance, it can explain why there is peak tropical upwelling on the summer-side equator (Rosenlof 1995). It could also help to explain the observed connection between boundary layer temperature anomalies and lower-stratospheric temperature anomalies, as well as the high correlations between tropical SST and the upwelling strength of the shallow BDC branch, which is observed on all time scales (Lin et al. 2015; Abalos et al. 2021). Numerical modeling suggests that strengthening of the subtropical jets changes the upward propagation of waves (Garcia and Randel 2008; Calvo et al. 2010; Shepherd and McLandress 2011), ultimately strengthening the wave-driven stratospheric upwelling, although the exact specifics seem to vary from model to model (Calvo et al. 2010; Simpson et al. 2011). In the zonally symmetric coupled troposphere–stratosphere theory analyzed in this work, an equatorial SST anomaly is not only associated with strengthening of the subtropical jets (which no doubt could change the subtropical distribution of wave drag in the real world), but also a strengthening of the tropopause geopotential. As such, the theory proposed in this work does not have to be mutually exclusive with those based on wave drag.

Besides the inclusion of a relaxational wave drag (shown to be a poor assumption), our work stays silent on how the momentum budget must change in order to balance changes in the meridional circulation (Ming et al. 2016b). However, there would undoubtedly be a large-scale wave response to steady tropospheric heating (Gill 1980). Thus, disentangling the effects of heating from the ensuing wave response is quite complicated, as the two occur in concert. While other studies have analyzed the wave response to tropospheric heating (Ortland and Alexander 2014; Jucker and Gerber 2017) (as well as its subsequent effects on the stratospheric circulation), we have instead focused on the *steady* response to tropospheric heating. In general, however, when tropical tropospheric heating is used to generate a wave response, it is difficult to separate the tropopause forcing mechanism described in this study from wave driving. For instance, Jucker and Gerber (2017) used idealized GCM simulations to show that the inclusion of a tropical warm pool significantly changed the annual-mean temperature of the tropical tropopause (and more importantly, more so than midlatitude land–sea contrast and orographic forcing). However, the imposition of a warm pool will both intensify the tropopause anticyclone over the region, and trigger a large-scale wave response. According to the analysis shown in this study, the increased tropopause geopotential will act to cool the tropopause and induce more upwelling (as would increased wave drag from the large-scale wave response). Separately, Ortland and Alexander (2014) forced equatorial waves by prescribing time-varying latent heating anomalies in a primitive equation model, and found that stationary waves and weakly westward-propagating waves are most responsible for driving residual-mean upwelling in the TTL. Again, tropospheric heating will induce a tropopause geopotential anomaly, such that the steady tropospheric forcing is not separated from the wave response. Regardless, both of the modeling results in Ortland and Alexander (2014) and Jucker and Gerber (2017) show that at least in numerical models, the seasonal cycle in upwelling in the tropical tropopause layer cannot be explained by tropospheric thermal forcing.

It is only fair for these conclusions to be discussed alongside the assumptions posited in this model. In this model, we assume that there is an instantaneous transition between tropospheric, quasi-equilibrium dynamics, and passive, dry stratospheric dynamics. In reality, the presence of the TTL could dampen the upward influence of tropospheric forcing. The assumption of a moist adiabatic lapse rate all the way to the tropopause is one that is has mixed observational evidence, which suggests that the free-tropospheric temperature anomalies, per degree of warming in the boundary layer, approximately follow a moist adiabat up to around 200 hPa, after which temperature anomalies transition to being out of phase with lower-tropospheric temperature anomalies (see Fig. 8 and Holloway and Neelin 2007) (though some of this may be owing to time averaging with a vertically moving tropopause). While the proposed theory can predict the magnitude of the tropopause temperature anomalies with respect to boundary layer warming, it does not include a transition layer. The presence of a transition layer could, in theory, dampen the vertical penetration of thermal forcing in the troposphere. This will be the subject of future research.

Finally, we also assume a fixed tropopause height that interfaces the two regimes, as in PE99. This makes the analysis mathematically tractable. Indeed, one would expect tropospheric temperature to affect tropopause height (Held 1982; Lin et al. 2017). The relaxation of both of these assumptions will be the subject of future research, but requires a theory for how moist convection interacts with the transition layer. More research is necessary to understand the role of convection in modulating the behavior of the transition layer.

The analysis carried out in section 4 uses the ERA5 dataset, which is not truly observational data. This could be mitigated by the use of GPS radio occultation (RO) measurements, provided by the COSMIC mission (Anthes et al. 2008). The high vertical resolution of GPS RO measurements could be leveraged in future work, as done in Grise and Thompson (2013). Furthermore, while we focused on large-scale tropospheric anomalies in this work, there are also numerous mesoscale convective systems, usually with anticyclones at their tops, that might also be able to contribute to tracer transport into the stratosphere. Higher-resolution observational data, such

as that provided by GPS RO measurements, could also be useful to evaluate this possibility.

Acknowledgments. The author thanks Adam Sobel and Peter Hitchcock for comments and suggestions on earlier versions of this work. The authors also thank two anonymous reviewers and Peter Haynes for their helpful suggestions, which greatly improved the manuscript. In particular, the authors are grateful for Peter Haynes's suggestions on the formulation of the coupled boundary condition. J. Lin gratefully acknowledges the support of the National Science Foundation through the NSF-AGS Postdoctoral Fellowship, under Award AGS-PRF-2201441.

Data availability statement. The monthly-mean ERA5 data for sea surface temperature are available at https://cds.climate.copernicus.eu/cdsapp#!/dataset/reanalysis-era5-single-levels-monthly-means via DOI: 10.24381/cds.f17050d7 (Hersbach et al. 2019b). The monthly averaged ERA5 data for temperature and geopotential are available at https://cds.climate.copernicus.eu/cdsapp#!/dataset/reanalysis-era5-pressure-levels-monthly-means via DOI: 10.24381/cds.6860a573 (Hersbach et al. 2019a). All code to generate the data from the theoretical models are available at https://github.com/linjonathan/steady_coupled_trop_strat.

APPENDIX

Details on Solutions

a. Solutions to conceptual model in section 2

The general solution to the homogeneous version of Eq. (9) [$q(z) = 0$] is

$$G(z) = A\exp(m_+ z) + B\exp(m_- z), \tag{A1}$$

where $m_\pm = 1 \pm \sqrt{1 + 4(k^2 + l^2)}/2$. Note, since $k^2 + l^2 > 0$, $m_+ > 0$ and $m_- < 0$ for all $k > 0$ and $l > 0$. We next define the Green's function, which satisfies

$$LG(z, \lambda) = \delta(z - \lambda), \tag{A2}$$

and is

$$G(z, \lambda) = \begin{cases} A\exp(m_+ z) + B\exp(m_- z), & \text{for } 0 < z < \lambda \\ C\exp(m_+ z) + D\exp(m_- z), & \text{for } \lambda < z < z_{\text{top}} \end{cases}, \tag{A3}$$

where z_{top} is assumed to be the top of the domain. The lower boundary condition requires that

$$A + B = \phi_T \tag{A4}$$

and the upper boundary condition requires that

$$Cm_+\exp(m_+ z_{\text{top}}) + Dm_-\exp(m_- z_{\text{top}}) = 0. \tag{A5}$$

Note that we choose to explicitly include z_{top} in Eq. (A5), since numerically evaluating the Green's functions requires $z_{\text{top}} < \infty$. Continuity of G across λ requires

$$A\exp(m_+\lambda) + B\exp(m_-\lambda) = C\exp(m_+\lambda) + D\exp(m_-\lambda), \tag{A6}$$

$$\lim_{\epsilon\to 0}\frac{\partial G}{\partial z}\bigg|_{z=\lambda-\epsilon}^{z=\lambda+\epsilon} - \lim_{\epsilon\to 0} G\big|_{z=\lambda-\epsilon}^{z=\lambda+\epsilon} = 1. \tag{A7}$$

Equations (A4)–(A7) are solved to obtain

$$A = \frac{\phi_T - \frac{1}{m_d}\left[\exp(-m_-\lambda) - \frac{m_+}{m_-}\exp(-m_+\lambda + m_d z_{\text{top}})\right]}{1 - \frac{m_+}{m_-}\exp(m_d z_{\text{top}})}, \tag{A8}$$

where

$$m_d = m_+ - m_- = \sqrt{1 + 4(k^2 + l^2)} > 0; \tag{A9}$$

B, C, and D are then obtained using Eqs. (A4)–(A6).

The Green's function can be convoluted with the source term (q) to obtain the geopotential:

$$\phi(z) = \int_0^\infty G(z, \lambda)q(\lambda)d\lambda. \tag{A10}$$

b. Numerical solver for coupled troposphere–stratosphere

In this section, we elaborate on the numerical solver of the coupled troposphere–stratosphere system [Eqs. (35) and (46)], given forcing in s^*. We approximate the meridional and vertical derivatives with second-order and sixth-order central finite differences, respectively. Since our specified s^* forcing is equatorially symmetric, we only have to discretize y from equator to pole, and impose a Neumann boundary condition at the equator. However, y appears in the denominator in both Eqs. (35) and (46). We circumvent this issue by numerically evaluating the equator at $\epsilon = 10^{-5}$ (three orders of magnitude smaller than the meridional grid spacing); y is evenly discretized from $y_{\max}$ to ϵ, where $y_{\max} = -10$. z is evenly discretized from the tropopause ($z^* = 1$) to the domain top, $z^*_{\text{top}} = 7$. The boundary conditions are

$$\phi(y = y_{\max}, z^*) = 0, \tag{A11}$$

$$\frac{\partial\phi}{\partial y}(y = \epsilon, z^*) = 0, \tag{A12}$$

$$\frac{\partial\phi}{\partial z}(y, z^* = z^*_{\text{top}}) = 0, \tag{A13}$$

as well as the aforementioned Eq. (46) on the boundary $z^* = 1$. The solutions are ensured to solve the original linear system of equations, as well as the boundary conditions, within numerical error. Finally, we use the findiff Python package to solve the system numerically (Baer 2018).

REFERENCES

Abalos, M., and Coauthors, 2021: The Brewer–Dobson circulation in CMIP6. *Atmos. Chem. Phys.*, **21**, 13 571–13 591, https://doi.org/10.5194/acp-21-13571-2021.

Andrews, D. G., J. R. Holton, and C. B. Leovy, 1987: *Middle Atmosphere Dynamics*. International Geophysics Series, Vol. 40, Academic Press, 489 pp.

Anthes, R. A., and Coauthors, 2008: The COSMIC/FORMOSAT-3 mission: Early results. *Bull. Amer. Meteor. Soc.*, **89**, 313–334, https://doi.org/10.1175/BAMS-89-3-313.

Baer, M., 2018: findiff software package. GitHub, https://github.com/maroba/findiff.

Birner, T., and H. Bönisch, 2011: Residual circulation trajectories and transit times into the extratropical lowermost stratosphere. *Atmos. Chem. Phys.*, **11**, 817–827, https://doi.org/10.5194/acp-11-817-2011.

Boehm, M. T., and S. Lee, 2003: The implications of tropical Rossby waves for tropical tropopause cirrus formation and for the equatorial upwelling of the Brewer–Dobson circulation. *J. Atmos. Sci.*, **60**, 247–261, https://doi.org/10.1175/1520-0469(2003)060<0247:TIOTRW>2.0.CO;2.

Butchart, N., 2014: The Brewer-Dobson circulation. *Rev. Geophys.*, **52**, 157–184, https://doi.org/10.1002/2013RG000448.

Calvo, N., R. R. Garcia, W. J. Randel, and D. R. Marsh, 2010: Dynamical mechanism for the increase in tropical upwelling in the lowermost tropical stratosphere during warm ENSO events. *J. Atmos. Sci.*, **67**, 2331–2340, https://doi.org/10.1175/2010JAS3433.1.

Chae, J. H., and S. C. Sherwood, 2007: Annual temperature cycle of the tropical tropopause: A simple model study. *J. Geophys. Res.*, **112**, D19111, https://doi.org/10.1029/2006JD007956.

Cohen, N. Y., E. P. Gerber, and O. Bühler, 2013: Compensation between resolved and unresolved wave driving in the stratosphere: Implications for downward control. *J. Atmos. Sci.*, **70**, 3780–3798, https://doi.org/10.1175/JAS-D-12-0346.1.

Danielsen, E. F., 1982: A dehydration mechanism for the stratosphere. *Geophys. Res. Lett.*, **9**, 605–608, https://doi.org/10.1029/GL009i006p00605.

Dima, I. M., and J. M. Wallace, 2007: Structure of the annual-mean equatorial planetary waves in the ERA-40 reanalyses. *J. Atmos. Sci.*, **64**, 2862–2880, https://doi.org/10.1175/JAS3985.1.

Dobson, G. M. B., 1956: Origin and distribution of the polyatomic molecules in the atmosphere. *Proc. Roy. Soc. London*, **236**, 187–193, https://doi.org/10.1098/rspa.1956.0127.

Emanuel, K. A., 1987: An air–sea interaction model of intraseasonal oscillations in the tropics. *J. Atmos. Sci.*, **44**, 2324–2340, https://doi.org/10.1175/1520-0469(1987)044<2324:AASIMO>2.0.CO;2.

——, 1994: *Atmospheric Convection*. Oxford University Press, 580 pp.

——, J. D. Neelin, and C. S. Bretherton, 1994: On large-scale circulations in convecting atmospheres. *Quart. J. Roy. Meteor. Soc.*, **120**, 1111–1143, https://doi.org/10.1002/qj.49712051902.

Fu, Q., 2013: Bottom up in the tropics. *Nat. Climate Change*, **3**, 957–958, https://doi.org/10.1038/nclimate2039.

——, C. M. Johanson, J. M. Wallace, and T. Reichler, 2006: Enhanced mid-latitude tropospheric warming in satellite measurements. *Science*, **312**, 1179, https://doi.org/10.1126/science.1125566.

Fueglistaler, S., M. Bonazzola, P. H. Haynes, and T. Peter, 2005: Stratospheric water vapor predicted from the Lagrangian temperature history of air entering the stratosphere in the tropics. *J. Geophys. Res.*, **110**, D08107, https://doi.org/10.1029/2004JD005516.

——, A. E. Dessler, T. J. Dunkerton, I. Folkins, Q. Fu, and P. W. Mote, 2009: Tropical tropopause layer. *Rev. Geophys.*, **47**, RG1004, https://doi.org/10.1029/2008RG000267.

Garcia, R. R., 1987: On the mean meridional circulation of the middle atmosphere. *J. Atmos. Sci.*, **44**, 3599–3609, https://doi.org/10.1175/1520-0469(1987)044<3599:OTMMCO>2.0.CO;2.

——, and W. J. Randel, 2008: Acceleration of the Brewer–Dobson circulation due to increases in greenhouse gases. *J. Atmos. Sci.*, **65**, 2731–2739, https://doi.org/10.1175/2008JAS2712.1.

Garfinkel, C. I., D. W. Waugh, L. D. Oman, L. Wang, and M. M. Hurwitz, 2013: Temperature trends in the tropical upper troposphere and lower stratosphere: Connections with sea surface temperatures and implications for water vapor and ozone. *J. Geophys. Res. Atmos.*, **118**, 9658–9672, https://doi.org/10.1002/jgrd.50772.

Garny, H., M. Dameris, W. Randel, G. E. Bodeker, and R. Deckert, 2011: Dynamically forced increase of tropical upwelling in the lower stratosphere. *J. Atmos. Sci.*, **68**, 1214–1233, https://doi.org/10.1175/2011JAS3701.1.

Gerber, E. P., 2012: Stratospheric versus tropospheric control of the strength and structure of the Brewer–Dobson circulation. *J. Atmos. Sci.*, **69**, 2857–2877, https://doi.org/10.1175/JAS-D-11-0341.1.

Gettelman, A., M. L. Salby, and F. Sassi, 2002: Distribution and influence of convection in the tropical tropopause region. *J. Geophys. Res.*, **107**, 4080, https://doi.org/10.1029/2001JD001048.

Gill, A. E., 1980: Some simple solutions for heat-induced tropical circulation. *Quart. J. Roy. Meteor. Soc.*, **106**, 447–462, https://doi.org/10.1002/qj.49710644905.

Grise, K. M., and D. W. J. Thompson, 2013: On the signatures of equatorial and extratropical wave forcing in tropical tropopause layer temperatures. *J. Atmos. Sci.*, **70**, 1084–1102, https://doi.org/10.1175/JAS-D-12-0163.1.

Haynes, P., 2005: Stratospheric dynamics. *Annu. Rev. Fluid Mech.*, **37**, 263–293, https://doi.org/10.1146/annurev.fluid.37.061903.175710.

——, and M. E. McIntyre, 1987: On the evolution of vorticity and potential vorticity in the presence of diabatic heating and frictional or other forces. *J. Atmos. Sci.*, **44**, 828–841, https://doi.org/10.1175/1520-0469(1987)044<0828:OTEOVA>2.0.CO;2.

——, and W. E. Ward, 1993: The effect of realistic radiative transfer on potential vorticity structures, including the influence of background shear and strain. *J. Atmos. Sci.*, **50**, 3431–3453, https://doi.org/10.1175/1520-0469(1993)050<3431:TEORRT>2.0.CO;2.

——, M. E. McIntyre, T. G. Shepherd, C. J. Marks, and K. P. Shine, 1991: On the "downward control" of extratropical diabatic circulations by eddy-induced mean zonal forces. *J. Atmos. Sci.*, **48**, 651–678, https://doi.org/10.1175/1520-0469(1991)048<0651:OTCOED>2.0.CO;2.

Held, I. M., 1982: On the height of the tropopause and the static stability of the troposphere. *J. Atmos. Sci.*, **39**, 412–417, https://doi.org/10.1175/1520-0469(1982)039<0412:OTHOTT>2.0.CO;2.

——, and A. Y. Hou, 1980: Nonlinear axially symmetric circulations in a nearly inviscid atmosphere. *J. Atmos. Sci.*, **37**, 515–533, https://doi.org/10.1175/1520-0469(1980)037<0515:NASCIA>2.0.CO;2.

Hersbach, H., and Coauthors, 2019a: ERA5 monthly averaged data on pressure levels from 1979 to present. C3S CDS, accessed

18 April 2019, https://cds.climate.copernicus.eu/cdsapp#!/dataset/reanalysis-era5-pressure-levels-monthly-means?tab=form.

——, and Coauthors, 2019b: ERA5 monthly averaged data on single levels from 1979 to present. C3S CDS, accessed 6 April 2023, https://cds.climate.copernicus.eu/cdsapp#!/dataset/reanalysis-era5-single-levels-monthly-means?tab=overview.

Hitchcock, P., T. G. Shepherd, and S. Yoden, 2010: On the approximation of local and linear radiative damping in the middle atmosphere. *J. Atmos. Sci.*, **67**, 2070–2085, https://doi.org/10.1175/2009JAS3286.1.

Holloway, C. E., and J. D. Neelin, 2007: The convective cold top and quasi equilibrium. *J. Atmos. Sci.*, **64**, 1467–1487, https://doi.org/10.1175/JAS3907.1.

Holton, J. R., P. H. Haynes, M. E. McIntyre, A. R. Douglass, R. B. Rood, and L. Pfister, 1995: Stratosphere-troposphere exchange. *Rev. Geophys.*, **33**, 403–439, https://doi.org/10.1029/95RG02097.

Jensen, E., and L. Pfister, 2004: Transport and freeze-drying in the tropical tropopause layer. *J. Geophys. Res.*, **109**, D02207, https://doi.org/10.1029/2003JD004022.

Johnson, R. H., and D. C. Kriete, 1982: Thermodynamic and circulation characteristics of winter monsoon tropical mesoscale convection. *Mon. Wea. Rev.*, **110**, 1898–1911, https://doi.org/10.1175/1520-0493(1982)110<1898:TACCOW>2.0.CO;2.

Jucker, M., and E. P. Gerber, 2017: Untangling the annual cycle of the tropical tropopause layer with an idealized moist model. *J. Climate*, **30**, 7339–7358, https://doi.org/10.1175/JCLI-D-17-0127.1.

Kerr-Munslow, A. M., and W. A. Norton, 2006: Tropical wave driving of the annual cycle in tropical tropopause temperatures. Part I: ECMWF analyses. *J. Atmos. Sci.*, **63**, 1410–1419, https://doi.org/10.1175/JAS3697.1.

Kiladis, G. N., K. H. Straub, G. C. Reid, and K. S. Gage, 2001: Aspects of interannual and intraseasonal variability of the tropopause and lower stratosphere. *Quart. J. Roy. Meteor. Soc.*, **127**, 1961–1983, https://doi.org/10.1002/qj.49712757606.

Kim, J., and S.-W. Son, 2012: Tropical cold-point tropopause: Climatology, seasonal cycle, and intraseasonal variability derived from COSMIC GPS radio occultation measurements. *J. Climate*, **25**, 5343–5360, https://doi.org/10.1175/JCLI-D-11-00554.1.

——, W. J. Randel, T. Birner, and M. Abalos, 2016: Spectrum of wave forcing associated with the annual cycle of upwelling at the tropical tropopause. *J. Atmos. Sci.*, **73**, 855–868, https://doi.org/10.1175/JAS-D-15-0096.1.

——, ——, and ——, 2018: Convectively driven tropopause-level cooling and its influences on stratospheric moisture. *J. Geophys. Res. Atmos.*, **123**, 590–606, https://doi.org/10.1002/2017JD027080.

Kuang, Z., and C. S. Bretherton, 2004: Convective influence on the heat balance of the tropical tropopause layer: A cloud-resolving model study. *J. Atmos. Sci.*, **61**, 2919–2927, https://doi.org/10.1175/JAS-3306.1.

Lin, J., and K. Emanuel, 2022: On the effect of surface friction and upward radiation of energy on equatorial waves. *J. Atmos. Sci.*, **79**, 837–857, https://doi.org/10.1175/JAS-D-21-0199.1.

Lin, P., Y. Ming, and V. Ramaswamy, 2015: Tropical climate change control of the lower stratospheric circulation. *Geophys. Res. Lett.*, **42**, 941–948, https://doi.org/10.1002/2014GL062823.

——, D. Paynter, Y. Ming, and V. Ramaswamy, 2017: Changes of the tropical tropopause layer under global warming. *J. Climate*, **30**, 1245–1258, https://doi.org/10.1175/JCLI-D-16-0457.1.

Ming, A., P. Hitchcock, and P. Haynes, 2016a: The double peak in upwelling and heating in the tropical lower stratosphere. *J. Atmos. Sci.*, **73**, 1889–1901, https://doi.org/10.1175/JAS-D-15-0293.1.

——, ——, and ——, 2016b: The response of the lower stratosphere to zonally symmetric thermal and mechanical forcing. *J. Atmos. Sci.*, **73**, 1903–1922, https://doi.org/10.1175/JAS-D-15-0294.1.

Norton, W. A., 2006: Tropical wave driving of the annual cycle in tropical tropopause temperatures. Part II: Model results. *J. Atmos. Sci.*, **63**, 1420–1431, https://doi.org/10.1175/JAS3698.1.

Orbe, C., and Coauthors, 2020: GISS model E2.2: A climate model optimized for the middle atmosphere—2. Validation of large-scale transport and evaluation of climate response. *J. Geophys. Res. Atmos.*, **125**, e2020JD033151, https://doi.org/10.1029/2020JD033151.

Ortland, D. A., and M. J. Alexander, 2014: The residual-mean circulation in the tropical tropopause layer driven by tropical waves. *J. Atmos. Sci.*, **71**, 1305–1322, https://doi.org/10.1175/JAS-D-13-0100.1.

Plumb, R. A., 2002: Stratospheric transport. *J. Meteor. Soc. Japan*, **80**, 793–809, https://doi.org/10.2151/jmsj.80.793.

——, and J. Eluszkiewicz, 1999: The Brewer–Dobson circulation: Dynamics of the tropical upwelling. *J. Atmos. Sci.*, **56**, 868–890, https://doi.org/10.1175/1520-0469(1999)056<0868:TBDCDO>2.0.CO;2.

Randel, W., and M. Park, 2019: Diagnosing observed stratospheric water vapor relationships to the cold point tropical tropopause. *J. Geophys. Res. Atmos.*, **124**, 7018–7033, https://doi.org/10.1029/2019JD030648.

——, R. R. Garcia, and F. Wu, 2002: Time-dependent upwelling in the tropical lower stratosphere estimated from the zonal-mean momentum budget. *J. Atmos. Sci.*, **59**, 2141–2152, https://doi.org/10.1175/1520-0469(2002)059<2141:TDUITT>2.0.CO;2.

——, F. Wu, and W. Rivera Ríos, 2003: Thermal variability of the tropical tropopause region derived from GPS/MET observations. *J. Geophys. Res.*, **108**, 4024, https://doi.org/10.1029/2002JD002595.

——, ——, H. Voemel, G. E. Nedoluha, and P. Forster, 2006: Decreases in stratospheric water vapor after 2001: Links to changes in the tropical tropopause and the Brewer-Dobson circulation. *J. Geophys. Res.*, **111**, D12312, https://doi.org/10.1029/2005JD006744.

——, R. Garcia, and F. Wu, 2008: Dynamical balances and tropical stratospheric upwelling. *J. Atmos. Sci.*, **65**, 3584–3595, https://doi.org/10.1175/2008JAS2756.1.

——, ——, N. Calvo, and D. Marsh, 2009: ENSO influence on zonal mean temperature and ozone in the tropical lower stratosphere. *Geophys. Res. Lett.*, **36**, L15822, https://doi.org/10.1029/2009GL039343.

Rosenlof, K. H., 1995: Seasonal cycle of the residual mean meridional circulation in the stratosphere. *J. Geophys. Res.*, **100**, 5173–5191, https://doi.org/10.1029/94JD03122.

Ryu, J.-H., and S. Lee, 2010: Effect of tropical waves on the tropical tropopause transition layer upwelling. *J. Atmos. Sci.*, **67**, 3130–3148, https://doi.org/10.1175/2010JAS3434.1.

Seviour, W. J. M., N. Butchart, and S. C. Hardiman, 2012: The Brewer–Dobson circulation inferred from ERA-Interim. *Quart. J. Roy. Meteor. Soc.*, **138**, 878–888, https://doi.org/10.1002/qj.966.

Shepherd, T. G., and C. McLandress, 2011: A robust mechanism for strengthening of the Brewer–Dobson circulation in response to climate change: Critical-layer control of subtropical

wave breaking. *J. Atmos. Sci.*, **68**, 784–797, https://doi.org/10.1175/2010JAS3608.1.

Sherwood, S. C., 2000: A stratospheric "drain" over the Maritime Continent. *Geophys. Res. Lett.*, **27**, 677–680, https://doi.org/10.1029/1999GL010868.

Simpson, I. R., T. G. Shepherd, and M. Sigmond, 2011: Dynamics of the lower stratospheric circulation response to ENSO. *J. Atmos. Sci.*, **68**, 2537–2556, https://doi.org/10.1175/JAS-D-11-05.1.

Sobel, A. H., and C. S. Bretherton, 2000: Modeling tropical precipitation in a single column. *J. Climate*, **13**, 4378–4392, https://doi.org/10.1175/1520-0442(2000)013<4378:MTPIAS>2.0.CO;2.

Taguchi, M., 2009: Wave driving in the tropical lower stratosphere as simulated by WACCM. Part I: Annual cycle. *J. Atmos. Sci.*, **66**, 2029–2043, https://doi.org/10.1175/2009JAS2854.1.

Vallis, G. K., 2017: *Atmospheric and Oceanic Fluid Dynamics*. Cambridge University Press, 946 pp.

Virts, K. S., and J. M. Wallace, 2014: Observations of temperature, wind, cirrus, and trace gases in the tropical tropopause transition layer during the MJO. *J. Atmos. Sci.*, **71**, 1143–1157, https://doi.org/10.1175/JAS-D-13-0178.1.

Yulaeva, E., J. R. Holton, and J. M. Wallace, 1994: On the cause of the annual cycle in tropical lower-stratospheric temperatures. *J. Atmos. Sci.*, **51**, 169–174, https://doi.org/10.1175/1520-0469(1994)051<0169:OTCOTA>2.0.CO;2.